Secure Compressed Sensing over Finite Fields

Some Results on Thermal Stress by Using Unified Formulation for Plates and Shells

E. Carrera * [†1], M. Cinefra [‡1], and F. A. Fazzolari [§2]

[1] *Politecnico di Torino, Corso Duca degli Abruzzi 24, 10129 , Torino, Italy.*
[2] *City University London, Northampton Square, London EC1V 0HB, United Kingdom.*

Submitted to : *Journal of Thermal Stresses*

Abstract

This work presents some results on two-dimensional modelling of thermal stress problems in multilayered structures. The governing equations are written by referring to the Unified Formulation (UF) introduced by the first author. These equations are obtained in a compact form, that doesn't depend on the order of expansion of variables in the thickness direction or the variable description (layer-wise models and equivalent single layers models). Classical and refined theories based on the Principle of Virtual Displacements (PVD) and advanced mixed theories based on the Reissner Mixed Variational Theorem (RMVT) are both considered. As a result, a large variety of theories are derived and compared. The temperature profile along the thickness of the plate/shell is calculated by solving the Fourier's heat conduction equation. Alternatively, thermo-mechanical coupling problems can be considered, in which the thermal variation is influenced by mechanical loading. Exact closed-form solutions are provided for plates and shells, but also the applications of the Ritz method and the Finite Element Method (FEM) are presented.

Keywords: thermal stress; coupled and uncoupled; Unified Formulation; plates and shells; Ritz formulation; Finite Element Method.

*Corresponding author: Tel: +39 0110906869, Fax: +44 0110906899, E-mail: erasmo.carrera.@polito.it
[†]Professor, Department of Mechanical and Aerospace Engineering.
[‡]Research Fellow ,Department of Mechanical and Aerospace Engineering.
[§]Ph.D. Candidate, School of Engineering and Mathematical Sciences.

1 Introduction

In the typical aeronautical structures such as multilayered composite plates and shells, the temperature variations are one of the most important factor for the stress fields that cause their failure. Advanced composite materials combine a number of properties, including high specific strength and stiffness, and nearly zero coefficient of thermal expansion in the fiber orientation. These relevant properties result in a growing use of composite materials in structures subjected to severe thermal environment, such as high temperatures, high gradients and cycling changes of temperature. Due to these implications, the effects of both high-temperature and mechanical loadings have to be considered in the design process of such structures [1], [2], [3]. An accurate description of local stress fields in the layers becomes mandatory to prevent thermally loaded structures failure mechanisms. For these reasons, increasing work has recently been devoted to the development of computational models for studying the behavior of high-temperature composite plates and shells [3].

Early [4],[5], and recent [6], [7] exact three dimensional solutions (3D) have shown that appropriate structural modelings are required to describe multilayered plates/shells with respect to traditional flat panels made of homogeneous isotropic materials. Transverse discontinuous mechanical properties cause, in fact, displacement fields $\boldsymbol{u} = (u_x, u_y, u_z)$ (bold letters denote arrays in a Cartesian reference system x, y, z) in the thickness direction z which can exhibit a rapid change of their slopes in correspondence to each layer interface. This is known as the *Zig-Zag* effects (ZZ). Nevertheless transverse stresses $\boldsymbol{\sigma}_n$=$(\sigma_{xz}, \sigma_{yz}, \sigma_{zz})$, for equilibrium reasons, must fulfill *Interlaminar Continuity* (IC) at each layer interface. $\boldsymbol{u}$ and $\boldsymbol{\sigma}_n$ have, in the most general case, discontinuous first derivatives with correspondence to each interface where the mechanical properties change. In [8] ZZ and IC were referred to as C_z^0–Requirements. The fulfillment of C_z^0–Requirements is a crucial point of two dimensional modeling of multilayered structures.

Many articles have appeared in which classical and advanced theories have been proposed and applied. Several reviews are available on this topic. Among these mention can be made of those by Tauchert [9], Noor and Burton [10], Argyris and Tenek [11] as well as that displayed in the book by Librescu [12], Thornton [13] and Reddy [14]. A discussion on those contributions which are related to the bending of anisotropic plates has already been provided in [15]. Some recent examples are discussed below. Accurate layer-wise theories were developed by Cho, Bert and Striz [16] and Murakami [17]; third order theory was used for each individual layer. According to Reddy [14] these type of theory in which the unknown variables are independent in each layer are herein denoted as Layer Wise Models (LWMs). Equivalent Single Layer Models (ELSMs), in which the unknown variables are the same for the whole plate, were proposed by: Ali, Bhaskar and Varadan [18] which used a cubic displacement field and Murakami Zig-Zag function for the in-plane displacement components and a parabolic expansion for the transverse displacement. Chattopaday and co-workers [19] developed a third order theory with constant and third order temperature distribution in the thickness direction whose extension to coupled thermo-piezoelectric

problems was given in [20].

In most of the available literature, the temperature profile $T(z)$ is assumed to be constant or linearly varying into the plate thickness direction z. On the other hand, as discussed by Tungikar and Rao [6], the form of $T(z)$ should be more conveniently taken as a result of solving the heat conduction problem. The interest on more realistic form of $T_(z)$ has been displayed by the works by Chattopaday and co-workers [19] and [20]. Furthermore, in [21], the author has clearly displayed that the employment of very accurate models could result inadequate unless accurate description of temperature profiles is made.

The thermoelastic problem, in which the temperature is accounted as an external load, has been defined in [22, 23] as partially coupled thermo-mechanical problem. Partially coupled thermo-mechanical models are extensively employed in the thermal stress analysis of aeronautical structures, where the temperature variations are one of the most important factors that can cause failure of the structures [1]-[3]. Several partially coupled models have been developed for the static analysis of multilayered plates [15], [21], [24] and shells [25]. However, these models cannot investigate the thermo-mechanical coupling effect in terms of frequencies, because they do not include the thermal term in the stiffness matrix. A fully coupled thermoelastic analysis, that considers both temperature and displacement fields as primary variables, permits to evaluate the effect of the temperature on the deformation and the changes in the temperature field due to the deformation [26].

In the recent past, the first author has studied the thermal effects in composite structures. In [21, 27] a study on the thermomechanical response of multilayered plates has been addressed. Partially coupled stress problems were considered by solving the Fourier's conductivity equation. The importance of mixed theories for a correct prediction of transverse shear/normal stresses due to thermal loadings have been remarked in [15]. Extensions to Functionally Graded Materials (FGMs) has been discussed in [24, 28].

This work presents several hierarchical two-dimensional models, obtained via Carrera's Unified Formulation (CUF) [29], for the thermal stress analysis of multilayered plates and shells. The governing equations are derived using both the Principle of Virtual Displacements(PVD) and the Reissner's Mixed Variational Theorem (RMVT). Closed form solutions, obtained via the Navier method, are presented for multilayered plates and shells. The applications of Ritz method [30]-[32] and the finite element method [33, 34] are also discussed. In the last part, partially coupled and fully coupled thermo-mechanical models are compared.

2 Classical plate/shell theories

The simplest known plate/shell theory is based on Kirchhoff assumptions, namely Classical Lamination Theory (CLT), see [14]. Transverse shear strains as well as transverse normal strains are neglected with

respect to the in-plane ones. In the framework of CLT applications, the displacement model can be written:

$$\begin{aligned} u_i = &\quad u_i^0 - z\, u_{z,_i} \quad i = x, y \\ u_z = &\quad u_z^0 \end{aligned} \tag{1}$$

where $i = x, y$ for plate geometry and $i = \alpha, \beta$ for shell geometry, being (α, β, z) the curvilinear coordinates reference system. For the sake of brevity, all models here described are referred to the plates, but they remain valid for shells if subscripts α, β are used in place of x, y. The superscript ^{0} denotes values of displacement on Ω which is the reference surface of the plate (usually the plate middle surface) Comma denotes partial derivatives.

The inclusion of transverse shear strains leads to the following form of previous equations.

$$\begin{aligned} u_i = &\quad u_i^0 + z\, \phi_i \quad i = x, y \\ u_z = &\quad u_z^0 \end{aligned} \tag{2}$$

This model is known as Reissner-Mindlin plate theory, namely First order Shear Deformation Theory, FSDT, see [14]. It consists of a first order Taylor–type expansion of displacement unknowns in the neighborhood of the reference surface Ω. ϕ_x, ϕ_y takes therefore the meaning of rotations of the normal to Ω in the two planes $x - z$ and $y - z$, respectively. These rotations can be also expressed in terms of transverse shear strains:

$$\phi_x = \epsilon_{xz} - u_{3,_x}, \quad \phi_y = \epsilon_{yz} - u_{3,_y}$$

FSDT displacement model can be put in compact form of Eqn.(4) according to the following notations:

$$\boldsymbol{u}(x, y, z) = \quad F_0(z)\, \boldsymbol{u}_0(x, y) \; + \; F_1(z)\, \boldsymbol{u}_1(x, y) \tag{3}$$

The polynomials assume the following values,

$$F_0(z) = 1, \; F_1(z) = z$$

while the displacement unknowns are:

$$u_{x_0}(x, y) = u_x^0, \; u_{y_0} = u_y^0, \; u_{z_0}(x, y,) = u_z^0, \;\; u_{x_1}(x, y) = \phi_x, \; u_{y_1} = \phi_y$$

and

$$u_{z_1}(x, y,) = 0 \tag{4}$$

3 Theories based on Unified Formulation

Carrera's Unified Formulation [29] represents in its classical formulation a generalization of that class of 2D and quasi-3D plate/shell theories based on axiomatic assumptions. Its accuracy has been proved in many applications ranging from multifield to aeroelastic problems. It turned out to be a powerful tool to deal with metallic and composite laminated beams, plates and shells. In the framework of CUF the displacement field is assumed as:

$$\mathbf{u} = \mathbf{F}_\tau \, \mathbf{u}_\tau, \qquad \tau = 0, 1, ..., N \tag{5}$$

where F_τ are functions of z and identify the kinematics description used for the displacement components. The functions $u_\tau = (u_{\tau_x}, u_{\tau_y}, u_{\tau_z})$ are the displacement vector components and N is the order of expansion. According to Einstein's notation, the repeated subscript τ indicates summation.

3.1 Higher order theories

Higher-order models are Equivalent Single Layer (ESL) models in which the displacement field is assumed for the whole laminate and a Taylor expansion is used as thickness functions.
Therefore, the displacement model is herein written in array form as:

$$\boldsymbol{u}(x, y, z) = \quad F_0(z) \, \boldsymbol{u}_0(x, y) \; + \; F_1(z) \, \boldsymbol{u}_1(x, y) + ... + ... \, F_N(z) \, \boldsymbol{u}_N(x, y) \tag{6}$$

where:

$$F_\tau(z) = z^\tau$$

FSDT model can be seen as a particular case of an ESL model with order of expansion $N = 1$ in which Eqn.(4) constraints is imposed. CLT results are in this work obtained by applying a penalty technique to the shear correction factor to FSDT analyses.

3.2 Introduction of Zig-Zag effects via Murakami ZZ function

The higher-order models are not able to describe the ZZ effect. The discontinuity of the first derivative with correspondence to the layer interfaces, in the ESL framework, can be introduced by employing the Murakami Zig-Zag function (MZZF) that was proposed in [35] in the framework of RMVT applications.

The Murakami Zig-Zag Functions $M(z)$ is defined according to the following formula [35]:

$$M(z) = (-1)^k \zeta_k \tag{7}$$

where the not dimensioned layer coordinate $\zeta_k = z_k/2h_k$ is introduced. z_k is the layer thickness coordinate and h_k is the thickness of the k-th layer.
$M(z)$ has the following properties: - It is piece-wise linear function of the layer coordinates z_k; - $M(z)$ has unit amplitude for the whole layers; - The slope $M'(z)=\frac{dM}{dz}$ assumes opposite sign between two-adjacent layers (its amplitude is layer thickness dependent).
The displacement field including MZZF is written in the form:

$$\boldsymbol{u} \;=\; \boldsymbol{u}_0 \;+\; (-1)^k \zeta_k \, \boldsymbol{u}_Z \;+\; z^r \, \boldsymbol{u}_r, \quad r = 1, 2, .., N \tag{8}$$

Subscripts $_Z$ refers to the introduced Zig-Zag term. Higher order distributions in the z-direction are introduced by the r-polynomials.

3.3 Introduction of Zig-Zag effect via Layer-Wise models

The Zig-Zag form of displacement distribution in the plate thickness directions can be acquired by using Layer-Wise models. Layer-wise description, in fact, requires assuming independent displacement variables in each k–layer. The Taylor expansion is not convenient for layer-wise description. Zig-Zag effects can be more conveniently imposed by employing interface values as unknown variables:

$$\boldsymbol{u}^k_{nM} = F_t \, \boldsymbol{u}^k_{nt} \;+\; F_b \, \boldsymbol{u}^k_{nb} \;+\; F_r \, \boldsymbol{u}^k_{nr} \;=\; F_\tau \, \boldsymbol{u}^k_{n\tau}, \qquad \tau = t, b, r, \quad r = 2, 3, .., N; \quad k = 1, 2, .., N_l \tag{9}$$

where N_l is the number of layers. It is intended that the subscripts t and b denote values related to the layer top and bottom surface, respectively. In fact, they consist of the linear part of the expansion. The thickness functions $F_\tau(\zeta_k)$ have been defined by:

$$F_t = \frac{P_0 + P_1}{2}, \quad F_b = \frac{P_0 - P_1}{2}, \quad F_r = P_r - P_{r-2}, \qquad r = 2, 3, .., N \tag{10}$$

in which $P_j = P_j(\zeta_k)$ is the Legendre polynomial of the j-order defined in the ζ_k–domain : -1 $\leq \zeta_k \leq$ 1. The chosen functions have the following properties:

$$\zeta_k = \begin{cases} 1 \;\; : \;\; F_t = 1; \quad F_b = 0; \quad F_r = 0 \\ -1 \;\; : \;\; F_t = 0; \quad F_b = 1; \quad F_r = 0, \end{cases} \tag{11}$$

The top and bottom values have been used as unknown variables. The interlaminar compatibility of displacement can be therefore easily linked:

$$\boldsymbol{u}_t^k = \boldsymbol{u}_b^{(k+1)}, \quad k = 1, N_l - 1 \tag{12}$$

3.4 Fulfillment of IC via RMVT applications

A possible manner to introduce the complete and a priori fulfillment of Zig-Zag and Interlaminar Continuity is to refer to RMVT application [36], [37]. According to RMVT statements both displacements $\boldsymbol{u}$ and transverse stresses $\boldsymbol{\sigma}_n = (\sigma_{xz}, \sigma_{yz}, \sigma_{zz})$ can be assumed. Formally, both Taylor and Legendre expansion discussed above can be used. In practice, see [37], transverse stress demands Legendre layer-wise expansion, while both expansion can be used for the displacements. In unified form displacement and stress fields are written as:

$$\boldsymbol{\sigma}_{nM}^k = F_t\, \boldsymbol{\sigma}_{nt}^k \;+\; F_b\, \boldsymbol{\sigma}_{nb}^k \;+\; F_r\, \boldsymbol{\sigma}_{nr}^k = F_\tau\, \boldsymbol{\sigma}_{n\tau}^k \qquad\qquad k = 1, 2, .., N_l \tag{13}$$

The top and bottom values have also been used as unknown variables. The interlaminar transverse shear and normal stress continuity can be therefore easily linked:

$$\boldsymbol{\sigma}_{nt}^k = \boldsymbol{\sigma}_{nb}^{(k+1)}, \quad k = 1, N_l - 1 \tag{14}$$

3.5 Classical and refined theories based on PVD

The classical displacement approach is formulated in terms of $\boldsymbol{u}^k$ via the principle of virtual displacements that in the static case and in presence of thermal stresses states:

$$\sum_{k=1}^{N_l} \int_{\Omega^k} \int_{A_k} \left(\delta {\boldsymbol{\epsilon}_{pG}^k}^T \left(\boldsymbol{\sigma}_{p\,H_d}^k - \boldsymbol{\sigma}_{p\,T}^k \right) + \delta {\boldsymbol{\epsilon}_{nG}^k}^T \left(\boldsymbol{\sigma}_{n\,H_d}^k - \boldsymbol{\sigma}_{n\,T}^k \right) \right) d\Omega^k dz \;=\; \delta L^e \tag{15}$$

δ is the variational symbol and subscript T denotes transposition of arrays. A_k and V denote the layer-thickness domain and volume; Ω^k is the layer middle surface bounded by Γ^k (Γ_g^k, Γ_m^k denotes those parts of Γ^k on which the geometrical and mechanical boundary conditions are prescribed, respectively). The variation of the internal work has been split into in-plane and out-of-plane parts and involves stress from Hooke's Law and strain from geometrical relations. δL_e is the virtual variation of the work made by the external layer-forces $\boldsymbol{p}^k = \{p_x^k, p_y^k, p_z^k\}$.

3.6 Advanced Mixed Theories based on RMVT

In the case of mixed plate theories, equilibrium and compatibility are both formulated in terms of the $\boldsymbol{u}^k$ and $\boldsymbol{\sigma}_n^k$ unknowns via Reissner's variational equation [36], [37]:

$$\sum_{k=1}^{N_l} \int_{\Omega^k} \int_{A_k} (\ \delta \boldsymbol{\epsilon}_{pG}^{k\,T} \ (\ \boldsymbol{\sigma}_{p\,H}^k - \boldsymbol{\sigma}_{p\,T}^k \ ) + \delta \boldsymbol{\epsilon}_{nG}^{k\,T} \ \boldsymbol{\sigma}_{n\,M}^k \ + \\ \delta \boldsymbol{\sigma}_{n\,M}^{k\,T} \ (\ \boldsymbol{\epsilon}_{nG}^k - \ (\ \boldsymbol{\epsilon}_{n\,H}^k \ - \ \boldsymbol{\epsilon}_{n\,T}^k \ ) \ ) \ ) d\Omega^k dz \ = \ \delta L^e \tag{16}$$

The first member of the equation includes the variations of the internal work in the plate: the first two terms come from the displacement formulation and lead to variationally consistent equilibrium conditions; the third 'mixed' term variationally enforces the compatibility of the transverse strain components.

3.7 Summary with acronyms of the considered theories

Depending on the type of formulation (PVD or RMVT), variables description (LW or ESLM), order of the used expansion etc., a number of two-dimensional theories can be constructed on the basis of the two-dimensional modelings described in this section. In order to concisely identify these theories, acronyms will be extensively used in the numerical parts.

In these acronyms, the first letter indicates the approach: equivalent single layer (E) or layer-wise (L). The second letter stands for the formulation: (D) for displacement formulation via PVD and (M) for mixed formulation via RMVT. This one can be followed by the letter (Z) if the Murakami function is used. The final number indicates the order of expansion. Therefore, one can have EDN, EDZN, LDN, EMN, EMZN or LMN theories.

4 The temperature profile in the thickness directions

A laminated plate, made of N_l orthotropic layers has been considered. a,b and h are the plate dimensions with respect to the defined coordinates. As done by Tungikar and Rao [6] the attention has been herein restricted to the particular case in which the multilayered plate is subjected to the following thermal boundary conditions:

$$\begin{aligned} &T = 0 && at \quad x = 0, \quad and \quad y = 0, b \\ &T = T_b \sin\left(\tfrac{m\pi}{a} x\right) \sin\left(\tfrac{m\pi}{b} y\right) && at \quad z = -\tfrac{h}{2} \\ &T = T_t \sin\left(\tfrac{m\pi}{a} x\right) \sin\left(\tfrac{m\pi}{b} y\right) && at \quad z = \tfrac{h}{2} \end{aligned} \tag{17}$$

m and n are the wave numbers along the plate width and length a and b, respectively.

Continuity conditions for the temperature and heat flux q_z in the thickness direction, at the each k–layer

interface is:

$$\begin{aligned} T^k &= T^{k+1} \\ q^k &= T^{k+1} \qquad k = 1, N_l - 1 \end{aligned} \tag{18}$$

Where the relation between flux and temperature is

$$q_z^k = K_3^k \frac{\partial T^k}{\partial z} \tag{19}$$

In which K_3=K_z represents the thermal conductivity of the k layer in the z-direction. The differential Fourier equation of heat conduction for the homogeneous orthotropic material, is

$$K_1 \frac{\partial^2 T}{\partial x^2} + K_2 \frac{\partial^2 T}{\partial y^2} + K_3 \frac{\partial^2 T}{\partial z^2} = 0 \tag{20}$$

where K_1 and K_2 are the thermal conductivities in the in–plane x, y directions, respectively.
The above set of governing equations can be solved according to the method described in [6] and [21]. The following temperature profiles is found for the k-th layer:

$$T_c(z) = T^k = (C_1^k \cosh s_1 z + C_2^k \sinh s_1 z) \sin \tfrac{m\pi}{a} x \sin \tfrac{m\pi}{b} y \tag{21}$$

The $2 \times N_l$ constant C_1^k, C_2^k are determined by imposing the previously written continuity conditions for flux q_z and the temperature at $N_l - 1$ interfaces, e.g. Eqn.(18) along with the two additional conditions on top-bottom surface for T.
In order to preserve consistency with the employed plate theories and without losing generality, the calculated temperature $T(z)$ given by Eqns.(21) has been expressed by using the same base function employed for transverse stress and displacement variables (see Sec 3),

$$T^k(x, y, z) = F_t \, T_t^k \; + \; F_b \, T_b^k \; + \; F_2 \, T_2^k = F_\tau \, T_\tau^k. \tag{22}$$

F_τ are a combination of Legendre polynomials either power of z.
By comparing the temperature profiles calculated in a three-layered structure for various thickness parameters (see Fig. 1), one can conclude that:

- The temperature distribution approach the linear case if and only if the thin plates cases are considered.
- The calculated temperature profiles of thick plates has an intrinsic layer-wise description.

The procedure to calculate the temperature profile in 'shell' structures is the same, but the the differential Fourier equation of heat conduction (20) takes into account also the curvature of the shell. For more

details, one can refer to the work [38].

5 Governing equations and closed-form solution

The C_z^0–requirements can be accounted by simply writing the governing equations at the multilayered level. First the equations (15) and (16) must be written in terms of unknown displacements and transverse stress variables. The necessary steps have been extensively explained in author's previous works [8], [37]. The governing equations for the displacement formulation are formally written

$$\boldsymbol{K}_d \ \boldsymbol{u} \ = \ \boldsymbol{p} \tag{23}$$

where the vector $\boldsymbol{p}$ includes thermal and mechanical loadings.
The corresponding boundary conditions are:

$$\boldsymbol{u} = \bar{\boldsymbol{u}} \quad or \quad \boldsymbol{\Pi}_d \ \boldsymbol{u} \ = \ \boldsymbol{\Pi}_d \ \bar{\boldsymbol{u}} \tag{24}$$

The governing system of differential equations at the multilayer level for the mixed cases is formally written in the following final form:

$$\begin{aligned} \boldsymbol{K}_{uu} \ \boldsymbol{u} + \boldsymbol{K}_{u\sigma} \ \boldsymbol{\sigma}_n \ &= \ \boldsymbol{p} \\ \boldsymbol{K}_{\sigma u} \ \boldsymbol{u} + \boldsymbol{K}_{\sigma\sigma} \ \boldsymbol{\sigma}_n \ &= 0 \end{aligned} \tag{25}$$

The boundary conditions are

$$\boldsymbol{u} = \bar{\boldsymbol{u}} \quad or \quad \boldsymbol{\Pi}_u \ \boldsymbol{u} + \boldsymbol{\Pi}_\sigma \ \boldsymbol{\sigma}_n = \boldsymbol{\Pi}_u \bar{\boldsymbol{u}} + \boldsymbol{\Pi}_\sigma \ \bar{\boldsymbol{\sigma}}_n + \boldsymbol{q}_\sigma^{1N_l} \tag{26}$$

The expanded expressions of the multilayer governing equations have been omitted for the sake of brevity. For more details, one can refer to [39].

5.1 Closed form solutions for harmonic distribution of temperature

Exact, closed form solutions of the derived system of differential equations that govern the thermo-mechanical response of a generally laminated multilayered plate, are not available. Approximate solution procedures could be conveniently implemented for this purpose [8]. The particular case in which the material has the following properties $\tilde{C}_{16} = \tilde{C}_{26} = \tilde{C}_{36} = \tilde{C}_{45} = 0$, has been considered here. In such a case, Navier-type closed form solutions can be found by assuming the following harmonic forms for the

applied mechanical and thermal loadings and unknown variables,

$$
\begin{gathered}
(u^k_{x_\tau}, \sigma^k_{xz_\tau}, p^k_{x_\tau}) = \textstyle\sum_{m,n} (U^k_{x_\tau}\ , S^k_{xz_\tau}\ , P^k_{x_\tau}\ ) \cos\frac{m\pi x}{a}\ \sin\frac{n\pi y}{b} \\
(u^k_{y_\tau}, \sigma^k_{yz_\tau}, p^k_{y_\tau}) = \textstyle\sum_{m,n} (U^k_{y_\tau}\ , S^k_{yz_\tau}\ , P^k_{y_\tau}\ ) \sin\frac{m\pi x}{a}\ \cos\frac{n\pi y}{b} \\
(u^k_{z_\tau}, \sigma^k_{zz_\tau}, p^k_{z_\tau}) = \textstyle\sum_{m,n} (U^k_{z_\tau},\ S^k_{zz_\tau},\ P^k_{z_\tau}\ ) \sin\frac{m\pi x}{a}\ \sin\frac{n\pi y}{b} \\
T(x,y,z) = T_P(z) \sin\frac{m\pi x}{a} \sin\frac{n\pi y}{b}
\end{gathered}
\tag{27}
$$

which correspond to simply-supported boundary conditions. m and n are wave numbers in the x and y directions, respectively. a and b are the plate width and length, respectively. The capital letters denote corresponding maximum amplitudes. Upon substitution of Eqns. (27), the governing equations written in the previous subsections assume the form of a linear system of algebraic equations, whose solutions are discussed in the next section.

Such assumptions remain valid for shells if (x, y) are substituted by the curvilinear coordinates (α, β).

6 Selected results for Plates

Most of the presented analyses refer to a thermo-mechanical problem for which the three–dimensional exact solution has recently been given by Bhaskar, Varadan and Ali [7]. Numerical results are presented for a cross–ply, symmetrically laminated [0°/90°/0°] square plate, in which the thermo-mechanical properties of the lamina are:

$$
E_L/E_T = 25,\ \ G_{LT}/E_T = .5,\ \ G_{TT}/E_T = .2,\ \ \nu_{LT} = \nu_{TT} = .25,
$$

$$
\alpha_T/\alpha_L = 1125,\ \ K_L = 36.42[W/mC^{-1}],\ \ K_T = .96[W/mC^{-1}]
$$

where L and T refer to directions parallel and perpendicular, respectively, to the fibers (see [14] for notations).

The deflection and stresses, if not differently declared, are presented in terms of the following dimensionless parameters:

$$
\bar{U}_z = hu_z/(\alpha_L T_0 a^2),\ \ \bar{S}_{ij} = \sigma_{ij}/(E_T \alpha_L T_0)
$$

6.1 Comparison of various theories to 3D exact solution

Table 1 compares the various theories to the 3D elasticity solution by Bhaskar and Varadan [7]. Transverse displacements and transverse shear stresses of thick and thin plates are compared. At the first

step, the temperature is assumed to linearly vary in the plate thickness direction, as in [7]. Results of 25 theories are given. The comparison made in [15] has been enlarged. Very different accuracy can be obtained by different plate theories. 23 theories have been, in fact, put between CLT (that is usually supposed to furnish the poorest description) and LM4 (that is supposed to give a quasi 3D description of stresses and displacement in laminated). Table 1, could be therefore used as a desk bed to assess available theories as well as future refinement of exiting theories. The following main comments can be made.

1. With some exception, theories merge for thin geometries.
2. Higher order expansions, e.g. N values, are requested to capture stress and displacement fields of thick plates.
3. The description of ZZ effect leads to significant improvements in both PVD and RMVT applications. In particular the Murakami Zig-Zag function improves very much the related results: EDZ analyses are more accurate than ED ones.
4. CLT and FSDT analyses can lead to large error to predict the thermal response of laminate plates.
5. The fulfillment of IC leads to improvements in the RMVT formulated theories.
6. LWMs descriptions are more accurate than corresponding ESLMs ones. On the other hand LWMs are more computational expensive with respect to ESLMs.
7. Mixed descriptions based on RMVT are more accurate than corresponding formulation based on PVD. That is the a priori fulfillment of IC leads to improved displacements and stresses.
8. RMVT is much more effective for ESLM formulations.
9. Different accuracy has been found for displacement evaluations with respect to transverse shear stress ones.
10. To be noticed the difficulties that theories with linear displacement fields in z, exhibit to consider a linear temperature profile. That happens for both thin and thick plates [15].
11. EDZ3 consists of the best ESLM multilayered theories in the framework of classical theories with only displacement unknowns and PVD applications.
12. EMZC3 consists of the best ESLM multilayered theories.
13. LM4 gives a quasi-3D description of displacement and stress fields of thermally loaded plates.
14. LD results, related to increasing N values, are very closed to corresponding LM ones.

6.2 Influence of temperature profile: comparison with assigned linear and calculated cases.

An exaustive comparison of different theories by considering assigned linear and calculated temperature profile is give in Tables 2 and 3 and Figures 2-4. The problem was in a more complete form discussed in [21]. Very thick (a/h=2), thick (a/h=4), moderately thick (a/h=10) and thin plates (a/h=100) have been considered. 3D solution for the calculated temperature profiles is not available. However, according to Table 1 analyses, LM4 results should be taken as a quasi-3D description also in the case of calculated temperature profiles. In addition to the comments of the previous section it should be noticed that:

1. The error introduced by the different theories is now also due to their capacity to capture the $T(z)$ profiles as they come from Eqn.(21).

2. The differences between T_a (assumed linear $T_P(z)$) and T_c (calculated $T_P(z)$) are extremely significant. In particular such a differences:

   - are very significant for both RMVT and PVD plate theories.
   - are larger for ESLMs with respect to LWMs.
   - increase very much for low values of N.
   - increase by thickness parameter decreasing.

3. 3D elasticity solutions which refer to linear $T_P(z)$ can be ineffective even though moderately thick plates are considered.

4. The differences above underlined should be related to the layer-wise form of T_c, as discussed in Sec. 5. Such a layer-wise form is difficult to be captured by ESL models as well as by lower order LW models.

5. The plots given in Figures 2-4 show that differences among several theories are very much subordinate to the considered position z. In particular, major discrepancies among the different theories exist with correspondence to the layer interfaces.

It is mainly concluded that an accurate thermal stress analysis could be meaningless unless the appropriate (calculated) temperature profile is considered.

7 Selected results for Shells

In this section three different benchmarks are discussed, these all have been provided by Khare et alii [40]. The first is a cylindrical shell (see Fig. 5) made of two carbon fiber reinforced layers with cross-ply orientation ($0°/90°$). The second and third case consist of spherical shell with a central soft core and

external carbon fiber reinforced layers; the case two has two external layers with the same orientation $0°$, while in the case three the soft core links two layers at the top with orientation $(90°/0°)$ and two layers at the bottom with orientation $(0°/90°)$. The notation for the geometry and the curvilinear reference system for shells with constant radii of curvature are indicated in Figure 5. Geometry and materials properties for the cylindrical shell are indicated in Table 4. Table 5 contains the data for the two considered spherical shells. The applied thermal load is due to a temperature distribution that varies in a bi-sinusoidal form in-the-plane and linear in the thickness direction:

$$\Delta T = (T_0 + \frac{z}{h}T_1)sin(\frac{m\pi}{a}\alpha)sin(\frac{n\pi}{b}\beta) \ . \tag{28}$$

Khare et alii [40] considers a zero mean value of temperature ($T_0 = 0$) and a gradient T_1 equal to 1. In this way the values of temperature at the top and at the bottom are $T_t = 0.5$ and $T_b = -0.5$, respectively. All the data are given for a correspondent environmental temperature which is a free parameter.
In the present ESL and LW models, the assigned linear distribution of temperature will be considered always LW. The distribution of temperature is always assumed linear through the multilayer to compare the proposed advanced models with those presented in [40] and [41]. The two models proposed in [40] consist of an equivalent single layer model with cubic expansion in the z direction for the three displacement components (named HOST12), and a first order shear deformation theory (called FOST). Khdeir et alii [41] proposed an higher order shear deformation theory (HSDT) for the benchmark one.
The Tables 6 and 7 consider the no-dimensional transverse displacement of the middle surface for the two-layered cylindrical shell. The present ESL models are compared with the HOST12 [40] and the HSDT [41] in Table 6. Third or fourth order of expansion (ED3 and ED4) are in good agreement with HOST12 and HSDT; low order of expansion in the thickness direction and classical models such as CLT and FSDT give an error larger than the 5% with respect to the ED4. The effect of the zig-zag Murakami's function is also investigated in the Table 6. Significant improvements are outlined for the ED1 with the use of zig-zag function (denoted as EDZ1): the error for the EDZ1 with respect to the ED4 is less than 1%. Finally, the layer wise analysis are reported in Table 7: if only the value of displacement in the middle is investigated, there are no significant improvements with respect to the ED4 (higher order of expansion); however the importance of LW models is clearly shown in the Figure 6 for the transverse shear stress σ_{xz}. Tables 8, 9 and Tables 10, 11 deal with for the spherical shell with lamination $0°/core/0°$ and $0°/90°/core/90°/0°$, respectively. The importance of layer wise models is evident in these tables and confirmed in the Figure 7. The benchmark $0°/core/0°$ shows an important difference between LD4 and ED4; such a difference is negligible in the benchmark $0°/90°/core/90°/0°$, due to the fact that the transverse displacement is considered in the middle of the core with very stiff faces. In this last benchmark there are two important considerations: -for low order of expansion the

LW models work better than the ESL ones, -LW models are mandatory to obtain a correct evaluation of the variables along the whole thickness direction. The effect of the curvature R/a has been investigated in each table, no remarkable differences have been found. The effect of the thickness ratio a/h is further illustrated in Tables 8 and 9. Conclusions already known for the plate geometries are confirmed.

8 Application of Ritz Method

In case of thermoelastic stability ad free vibration analysis, the Principle of Virtual Displacement (PVD) can be written in the following form:

$$\sum_{k=1}^{N_l} \int_{\Omega^k} \int_{A^k} \left(\delta \boldsymbol{\varepsilon}_{pG}^{k\,T} \, \boldsymbol{\sigma}_{pC}^{k} \, + \, \delta \boldsymbol{\varepsilon}_{nG}^{k\,T} \, \boldsymbol{\sigma}_{nC}^{k} \right) \mathrm{d}\Omega^k \, \mathrm{d}z \, = \sum_{k=1}^{N_l} \delta L_{ext}^{k} - \sum_{k=1}^{N_l} \delta L_{F_{in}}^{k} \tag{29}$$

The PVD is a useful tool to obtain both strong and weak forms of the governing equations. Approximation methods embedded within the framework of CUF have been accurately described and validated in [42]-[44]. The combination of the advanced plate/shell models hierarchically generated via CUF with the Ritz method based on the choice of trigonometric trial functions leads to the Hierarchical Trigonometric Ritz Formulation (HTRF) extensively employed in static and dynamics analysis of laminated composite plates and shells.

8.1 The Hierarchical Trigonometric Ritz Formulation

The HTRF is hereafter developed following some steps which lead to the Ritz governing equations for thermoelastic stability and free vibration analysis. In the Ritz method the displacement amplitude vector $\mathbf{u}_{\tau}^{k}$, which individuates the maximum amplitude in the oscillation, that maximizes the related energies, is expressed in series expansion as:

$$\mathbf{u}_{\tau}^{k} = \mathbf{U}_{\tau i}^{k} \, \boldsymbol{\Psi}_i \qquad \text{where} \quad i = 1, ..., \mathcal{N} \quad \tau = \tau_{u_x}, \tau_{u_y}, \tau_{u_z} \tag{30}$$

$\mathcal{N}$ indicates the order of expansion in the approximation. Consequently the harmonic displacement field, in compact way, assumes the following form:

$$\mathbf{u}^{k} = \mathbf{F}_{\tau} \, \mathbf{U}_{\tau i}^{k} \, \boldsymbol{\Psi}_i \tag{31}$$

where:

$$\mathbf{U}_{\tau i}^{k} = \begin{bmatrix} U_{x\tau_{u_x} i}^{k}\, e^{\imath\,\omega_{ij}\,t} \\ U_{y\tau_{u_y} i}^{k}\, e^{\imath\,\omega_{ij}\,t} \\ U_{z\tau_{u_z} i}^{k}\, e^{\imath\,\omega_{ij}\,t} \end{bmatrix}, \quad \mathbf{\Psi}_i = \begin{bmatrix} \psi_{x_i} & 0 & 0 \\ 0 & \psi_{y_i} & 0 \\ 0 & 0 & \psi_{z_i} \end{bmatrix}, \quad \mathbf{F}_\tau = \begin{bmatrix} F_{\tau_x} & 0 & 0 \\ 0 & F_{\tau_y} & 0 \\ 0 & 0 & F_{\tau_z} \end{bmatrix} \tag{32}$$

$U_{x\tau_{u_x} i}^{k}$, $U_{y\tau_{u_y} i}^{k}$, $U_{z\tau_{u_z} i}^{k}$ are the unknown coefficients, ψ_{x_i}, ψ_{y_i}, ψ_{z_i} are the trial functions appropriately chosen on the type of problem. Different expansions F_τ are used for the three components (u_x, u_y, u_z) with orders of expansion $N_{u_x}, N_{u_y}, N_{u_z}$, respectively. The results are strongly dependent on the functions that will be chosen. Convergence to the exact solution is guaranteed if the basis functions are admissible functions [14, 42, 44].

By writing the stresses and strains in function of displacements (30), one obtains the following quadratic forms of the internal work, the work done by the inertial forces and work done by the external forces:

$$\delta L_{int}^{k} = \delta \mathbf{U}_{\tau i}^{k^T} \mathbf{K}^{k\tau sij} \mathbf{U}_{sj}^{k}, \qquad \delta L_{F_{in}}^{k} = \delta \mathbf{U}_{\tau i}^{k^T}\, \mathbf{M}^{k\tau sij}\, \ddot{\mathbf{U}}_{sj}^{k}, \qquad \delta L_{ext}^{k} = \delta \mathbf{U}_{\tau i}^{k^T} \mathbf{K}_{\sigma}^{k\tau sij} \mathbf{U}_{sj}^{k} \tag{33}$$

The explicit expressions of the Ritz stiffness ($\mathbf{K}$), mass ($\mathbf{M}$) and initial stress ($\mathbf{K}_\sigma$) matrices can be found in [30, 42]. The PVD in Eq. (29) corresponds to the minimization of the total energy of the system which leads to the discrete form of the governing differential equations:

$$\delta \mathbf{U}_{\tau i}^{k^T} : \qquad \left[\left(\mathbf{K}^{k\tau sij} + \mathbf{K}_{\sigma}^{k\tau sij} \right) - \omega_{ij}^{2} \mathbf{M}^{k\tau sij} \right] \mathbf{U}_{sj}^{k} = 0 \tag{34}$$

The free-vibration response of the multylayered plate, under combined thermal and mechanical loadings, leads to the following eigenvalues problem:

$$\left\| \left(\mathbf{K}^{k\tau sij} + \mathbf{K}_{\sigma}^{k\tau sij} \right) - \omega_{ij}^{2}\, \mathbf{M}^{k\tau sij} \right\| = 0 \tag{35}$$

When a thermo-mechanical buckling analysis is performed, the mass contribution is discarded and the eigenvalues problem can be reformulated as follows:

$$\left\| \mathbf{K}^{k\tau sij} + \lambda_{ij}\, \mathbf{K}_{\sigma}^{k\tau sij} \right\| = 0 \tag{36}$$

8.2 Results

Results have been obtained considering simply supported plates, materials in Tables 12 and 13 and trigonometric trial functions following defined:

$$\begin{aligned}
\psi_{x_{mn}}(x,y) &= \sum_m \sum_n \cos\left(\frac{m\,\pi\,x}{a}\right) \sin\left(\frac{n\,\pi\,y}{b}\right) \\
\psi_{y_{mn}}(x,y) &= \sum_m \sum_n \sin\left(\frac{m\,\pi\,x}{a}\right) \cos\left(\frac{n\,\pi\,y}{b}\right) \\
\psi_{z_{mn}}(x,y) &= \sum_m \sum_n \sin\left(\frac{m\,\pi\,x}{a}\right) \sin\left(\frac{n\,\pi\,y}{b}\right)
\end{aligned} \tag{37}$$

Using trigonometric functions the surface integrals present in the governing equations can be solved analitically by means of symbolic computation (MATEMATICA or MAPLE softwares). Some results in Table 14 obtained by employing the HTRF are compared to those given by Galerkin and Generalized Galerkin methods developed in [42]. In this respect, it is useful to note that trigonometric functions are of class ∞, then in this particular case it is not relevant that Galerkin method require an higher order of differentiability. Results will be given using the acronyms system presented in [30]. The ESL theories are indicated as $ED_{N_{u_x} N_{u_y} N_{u_z}}$ where E means the ESL approach, D means that the PVD has been employed. Similarly the acronym used to describe the zig-zag theories is $EDZ_{N_{u_x} N_{u_y} N_{u_z}}$, where Z states that Murakami's function has been included in the ESL displacement field. LW theories are defined as $LD_{N_{u_x} N_{u_y} N_{u_z}}$ where L indicates that a layer-wise approach has been used..

8.2.1 Convergence analysis for pure thermal and pure mechanical buckling loads, for symmetric angle-ply laminates

The convergence analysis is a crucial point when approximate solutions are required. From a theoretical point of view once proved that the trial functions are admissible in the original variational principle, the convergence to the true solution is guaranteed as the number of admissible functions tends to infinity. In practical computations, the number of Ritz and/or Galekin terms is limited by CPU time this truncation inevitably affects the results accuracy. Furthermore, another related aspect to take into account is the stability of the solution, since numerical error my occur due to the ill conditioning when many admissible functions are required to obtain a good convergence. All these reasons justify the importance to carry out a convergence analysis whenever an approximate solution is applied. In Table 14 convergence analysis, in the case of pure thermal buckling loads is performed by using a ED_{222} model and Ritz (R), Galerkin (G) and Generalized Galerkin (GG) approximation methods. A four layers laminate $[\theta/-\theta]_{\mathrm{s}}$ made of MAT-1 (AS4/3502) is investigated. A good convergence, for all the employed methodologies, is reached by using $M = N = 12$ as half-waves number. Note that a square selection strategy is adopted, i.e., the same number of Ritz or Galekin terms is used in the expansion along x and y directions. GM has an higher

rate of convergence which leads to higher critical temperature when compared to R and GGM. This difference, between GM and GGM, is due to the non-zero boundary terms in angle-ply laminates. The latters are retained in the GGM and discarded in the GM. When isotropic plates or cross-ply laminates are studied than the three methodologies lead to the same results (see [42] for further details). In this case the influence of the boundary terms is strongly dependent both from the half-waves number and from the lamination angles. In Table 15 pure thermal and pure buckling loads for several refined plate theories are shown. Different lamination angles and in-plane load combinations are investigated using $M = N = 12$ as half-waves number in the series expansion. In particular axial, biaxial, pure shear and combined compressive and shear loads have been considered. The LD_{222} model represents, in this analysis, the best trade off between results accuracy and computational CPU time.

8.2.2 Influence of significant parameters on the critical temperature of regular symmetric angle-ply laminates

A five layers laminate, with stacking sequence $[\theta/-\theta/\theta/-\theta/\theta]$ and MAT-3 has been analyzed from Fig. 8 trough Fig. 11. In Fig. 8 the influence of the lamination angle and the variable kinematics are shown, as can be observed, $\theta = 45°$ is the right choose to maximize the critical temperature parameters $\lambda_\vartheta = \alpha_0 \, \mathrm{T}_{cr}$ and as anticipated the LD_{222} model is the theory used to investigate thin and thick plates due to its efficiency and accuracy. As shown in Fig. 9 increasing the orthotropic ratio, λ_ϑ increases as well. It's interesting to note that once fixed the aspect ratio $a/b = 2$, varying the lamination angle, the angle which maximize λ_ϑ is significantly dependent on the thickness ratio, in particular for thin laminate $(a/h = 100)$, $\theta = 60°$, for thick laminate $(a/h = 10)$, $\theta = 50°$. The influence of the thickness ratio on λ_ϑ is clearly shown in Fig. 11.

9 Application of FEM

According to the Finite Element Method (FEM), the unknown variables of the problem are expressed in terms of their nodal values, via the shape functions N_i:

$$\mathbf{u}^k_\tau(x, y) = N_i \, \mathbf{q}^k_{\tau i} \quad i = 1, 2, \ldots, N_n \tag{38}$$

$$\boldsymbol{\sigma}^k_{n\tau}(x, y) = N_i \, \mathbf{f}^k_{\tau i} \quad i = 1, 2, \ldots, N_n \tag{39}$$

where N_n denotes the number of nodes of the element while:

$$\mathbf{q}^k_{\tau i} = \begin{bmatrix} q^k_{u_x \tau i} \\ q^k_{u_y \tau i} \\ q^k_{u_z \tau i} \end{bmatrix} \qquad \mathbf{f}^k_{\tau i} = \begin{bmatrix} f^k_{\sigma_{xz} \tau i} \\ f^k_{\sigma_{yz} \tau i} \\ f^k_{\sigma_{zz} \tau i} \end{bmatrix} \tag{40}$$

Substituting eqs.(38) and (39) respectively in eqs.(5) and (13), the final expressions of the displacement field and transverse stresses can be obtained:

$$\mathbf{u}^k(x,y,z) = F_\tau \, N_i \, \mathbf{q}^k_{\tau i} \tag{41}$$

$$\boldsymbol{\sigma}^k_n = F_\tau \, N_i \, \mathbf{g}^k_{\tau i} \tag{42}$$

As regard the temperature, the generic $\theta^k_\tau(x,y)$can be written:

$$\theta^k_\tau(x,y) = t \, A^k_\tau \tag{43}$$

where t takes into account the in-plane shape of the imposed temperature for the uncoupled problem while $t = 0$ for the fully coupled one. Now expressing A^k_τ in terms of the nodal values of the temperature via the shape functions:

$$A^k_\tau = N_i \, a^k_{\tau i} \quad i = 1, 2, \ldots, N_n \tag{44}$$

and putting together eqs.(22),(44) and (43), the temperature discretization takes the form:

$$\theta^k(x,y,z) = F_\tau \, t \, N_i \, a^k_{\tau i} \tag{45}$$

The thermoelastic analysis of multilayered plates and shells can be done using both the PVD (15) and RMVT (16) variational statement. The governing equations for the the classical *Principle of Virtual Displacement* state:

$$\delta {\mathbf{q}^k_{\tau i}}^T : \qquad \mathbf{K}^{k\tau sij}_{uu} \, \mathbf{q}^k_{sj} \, = \, \mathbf{K}^{k\tau sij}_{u\theta} \, \mathbf{a}^k_{sj} \tag{46}$$

while for the mixed formulation *RMVT*:

$$\begin{aligned} &\delta {\mathbf{q}^k_{\tau i}}^T : \qquad \mathbf{K}^{k\tau sij}_{uu} \mathbf{q}^k_{sj} + \mathbf{K}^{k\tau sij}_{u\sigma} \mathbf{f}^k_{sj} = \mathbf{K}^{k\tau sij}_{u\theta} a^k_{sj} \\ &\delta \mathbf{f}^{kT}_{\tau i} : \qquad \mathbf{K}^{k\tau sij}_{\sigma u} \mathbf{q}^k_{sj} + \mathbf{K}^{k\tau sij}_{\sigma\sigma} \mathbf{f}^k_{sj} = \mathbf{K}^{k\tau sij}_{\sigma\theta} a^k_{sj} \end{aligned} \tag{47}$$

After the application of the appropriate boundary conditions, eqs.(46),(47) can be solved. For more details, one can refer to the work [33].

9.1 Results

Numerical results are then presented for two cases:

1. Simply supported square plate loaded with a bi-sinusoidal temperature field given by:

$$\theta = \frac{2\,\theta_M\,z}{h}\sin\frac{\pi\,x}{a}\sin\frac{\pi\,y}{b}$$

2. Simply supported square plate loaded with the temperature distribution based on heat conduction model where $\theta(z)$ is given by eq.(22)

a and b are the dimensions of the plate along x-axis and y-axis respectively while h is its thickness and θ_M is the value of the temperature at the top surface of the plate.
The laminate presents three layers (stacking sequence [0/90/0]) made of unidirectional laminae with a thickness of $h_k = \frac{h}{3}$ and their mechanical and thermal properties are:

$$\frac{E_L}{E_T} = 25 \qquad \frac{G_{LT}}{E_T} = 0.5 \qquad \frac{G_{TT}}{E_T} = 0.2$$

$$\nu_{LT} = \nu_{TT} = 0.25 \qquad \frac{\alpha_T}{\alpha_L} = 1125$$

$$\kappa_L = 36\frac{W}{m^\circ C} \qquad \kappa_T = 0.96\frac{W}{m^\circ C}$$

where E and G are the Young and shear moduli while the subscripts L and T refer to directions parallel and perpendicular to the fibers. The displacements and stresses in critical in-plane and thickness location are presented for four different thickness ratios $S = \frac{a}{h} = 4, 10, 20, 100$. Deflections and stresses are presented in terms of the following dimensionless parameters:

$$\bar{w} = \frac{w}{h\,\alpha_L\theta_M\,S^2} \qquad (\bar{u}\,,\,\bar{v}) = \frac{(u\,,\,v)}{h\,\alpha_L\theta_M\,S} \qquad (\bar{\sigma}_i) = \frac{\sigma_i}{E_T\,\alpha_L\,\theta_M\,S} \tag{48}$$

The results are relative to a plate discretized with $[6 \times 6]$ 9 node elements; this configuration has been chosen after that a convergence analysis was performed. The results of the convergence analysis are summarized in table 16.
The values of the dimensionless transversal displacement w are listed in tables (17) and (18) for the assumed and calculated temperature profile respectively. Other results in terms of in-plane displacements and stresses are shown in Fig. 12 for calculated profile.
Figures 13(a),13(b) present a comparison between the results of the dimensionless displacement field

and the transverse stresses for both the linear and the actual temperature profile and different side-to-thickness ratios (S=4 and S=10). A few considerations on the obtained results follow:

1. all the FEs match very well the analytical solution. All the FEs lead to accurate results with respect to the exact solution for all the thickness ratios except for LD1 and ED1 element. In fact, plate elements that present a constant transverse normal strain such as LD1 and ED1 lead to inaccurate results for both thick and thin plates. It is confirmed what found in [15], [21]: at least a parabolic expansion for the displacements (u_x, u_y and u_z components) is required to capture the linear thermal strains that are related to a linear through-the-thickness temperature distribution.

2. In general layerwise theories performed better than equivalent single layer ones and often also with a lower order of the expansion of the unknowns.

3. Equivalent single layer analyses are quite satisfactory only if applied to thin plates (S=100). On the other hand, higher order results are very good for all the thickness ratios but require a lot more of computational time.

4. LD4 and LM4 results matches perfectly the displacements obtained from the exact solution and the analytical implementation of the unified formulation.

5. The use of mixed models is mandatory for an accurate description of the transverse stresses in particular for the higher thickness ratios.

6. Several difficulties have been found in the recovery of the normal stress; only LM4 model gives acceptable results.

7. In the calculated temperature profile case, a general agreement of the numerical results with the analytical ones has been found for LW FEs and higher thickness ratios.

8. The solution of the heat conduction problem has shown that thick plates present a temperature profile that can considerably differ from the mostly assumed linear form, thus, calculated and assumed temperature profiles lead to very different responses.

9. Figures 13(a),13(b) demonstrate how the choice of the calculated temperature profile instead of the simple constant one is mandatory for thickness ratios lower than 10.

10 Coupled thermo-mechanical problems

A fully coupled thermoelastic variational statement is obtained by virtue of an extension of the principle of the virtual displacement (PVD), which takes into account the internal thermal virtual work. By

considering a laminate of N_l layers, the variational statement can be written as:

$$\sum_{k=1}^{N_l} \int_{\Omega_k} \int_{A_k} \left(\delta \boldsymbol{\varepsilon}_{pG}^{k^T} \boldsymbol{\sigma}_{pC}^k + \delta \boldsymbol{\varepsilon}_{nG}^{k^T} \boldsymbol{\sigma}_{nC}^k - \delta\theta^k \, \eta_C^k - \delta \boldsymbol{\vartheta}_{pG}^{k^T} \boldsymbol{h}_{pC}^k - \delta \boldsymbol{\vartheta}_{nG}^{k^T} \boldsymbol{h}_{nC}^k \right) \mathrm{d}\Omega_k \, \mathrm{d}z = \sum_{k=1}^{N_l} \delta L_e^k - \sum_{k=1}^{N_l} \delta L_{F_{in}}^k \tag{49}$$

where the δL_e^k and $\delta L_{F_{in}}^k$ are the external and inertial virtual works at the k-layer level, respectively. When a gradient of temperature variation does not exist, the terms $\left(\delta \boldsymbol{\vartheta}_{pG}^{k^T} \boldsymbol{h}_{pC}^k \right)$ and $\left(\delta \boldsymbol{\vartheta}_{nG}^{k^T} \boldsymbol{h}_{nC}^k \right)$ are neglected in the variational statement in Eq. (49). Under these hypotheses the coupled thermoelastic variational statement becomes:

$$\sum_{k=1}^{N_l} \int_{\Omega_k} \int_{A_k} \left(\delta \boldsymbol{\varepsilon}_{pG}^{k^T} \boldsymbol{\sigma}_{pC}^k + \delta \boldsymbol{\varepsilon}_{nG}^{k^T} \boldsymbol{\sigma}_{nC}^k - \delta\theta^k \, \eta_C^k \right) \mathrm{d}\Omega_k \, \mathrm{d}z = \sum_{k=1}^{N_l} \delta L_e^k - \sum_{k=1}^{N_l} \delta L_{F_{in}}^k \tag{50}$$

In Eqs. (49) and (50) the first variation represents a minimization condition with respect to the primary variables, namely, displacements and temperature unknowns. The FEM governing equations are directly obtained using the variational statement in Eq. (50) (see [34] for a complete overview) and they state:

$$\begin{aligned} \delta \mathbf{U}_{\tau i}^{k^T} : \quad & \mathbf{K}_{u\,u}^{k\tau sij} \, \mathbf{U}_{sj}^k + \mathbf{K}_{u\,\theta}^{k\tau sij} \, \boldsymbol{\Theta}_{sj}^k = -\mathbf{M}_{u\,u}^{k\tau sij} \, \ddot{\mathbf{U}}_{sj}^k \\ \delta \boldsymbol{\Theta}_{\tau i}^{k^T} : \quad & \mathbf{K}_{\theta\,u}^{k\tau sij} \, \mathbf{U}_{sj}^k + \mathbf{K}_{\theta\,\theta}^{k\tau sij} \, \boldsymbol{\Theta}_{sj}^k = 0 \end{aligned} \tag{51}$$

10.1 Assessment of temperature profile, steady-state solution

A simply supported three-layered square plate of edge $a = 0.1$ $[m]$ is considered. The top and bottom layer are made of aluminium, having equal thickness h_1. The middle layer is made of steel and has thickness $2 \times h_2$. Aluminium material properties are $E = 73.0E9$ $[Pa]$, $G = 27.239E9$ $[Pa]$, $\nu = 0.34$, $\alpha = 25.D - 6$ $[K^{-1}]$, $\kappa = 180$ $[W/(m \cdot K)]$, $\rho = 2800$ $[kg/m^3]$ and $C = 897$ $J/(K \cdot kg)$, where α is the coefficient of thermal expansion. Steel coefficients are $E = 210.0E9$ $[Pa]$, $G = 80.77E9$ $[Pa]$, $\nu = 0.3$, $\alpha = 11.1E - 6$ $[K^{-1}]$, $\kappa = 13$ $[W/(m \cdot K)]$, $\rho = 7860$ $[kg/m^3]$, $C = 450$ $J/(K \cdot kg)$. The T_{ref} is set to 298.15 $[K]$. A temperature variation respect to T_{ref} is imposed at the top and at the bottom face of the panel: $+10$ $[K]$ and -10 $[K]$ respectively. A coupled thermo-mechanical static analysis was run with a regular mesh of 11×11 Q4 LD1 FEs to calculate the through-the-thickness temperature profile and the plate displacement caused by the imposed temperatures, at steady-state condition. The attention is restricted to the central point of the plate $(\frac{a}{2}, \frac{a}{2})$. Each curve in Fig. 14 shows a temperature profile along the thickness of the plate. Different geometrical configurations are considered by the variation of h_1 and h_2 mutual dimensions, keeping the same total thickness. The calculated temperatures profiles are in very good agreement with the exact solution obtained applying Fourier's law (interface points θ_{exact}). The middle plate displacement u_z is illustrated in Fig. 15 for the various choices of h_1/h_2 ratios. The

configuration of minimum displacement is identified by the minimum of the curve. Fig. 16 shows the variation of the temperature profile when κ_2 varies progressively from the value typical of steel to the value typical of aluminium. The agreement with the exact solution is reconfirmed. Moreover, if $\kappa_1 = \kappa_2$ the temperature profile is linear, as usual for a single-layered panel.

Concluding, the results show the usefulness of the formulated thermo-mechanical FEs, which permit to calculate in one single run the steady-state static deformation of a structure subjected to thermal loading. The separate application of the Fourier's law to obtain the through-the-thickness temperature profile is not required. In fact, the temperature distribution through all the layers of the structure is automatically calculated by using the material thermal conductivity coefficients, which are considered together with the other constitutive coefficients in the governing equations.

11 Conclusions

The paper has compared refined and advanced theories based on CUF for the analysis of the thermo-mechanical response of multilayered plates and shells. Coupled and uncoupled problems have been considered. In the latter case, the temperature profile along the thickness was both assumed linear or calculated by solving the heat conduction equation.

The following main conclusions can be made.

1. An accurate description of the stress and displacement fields can be meaningless unless an accurate description is made of the temperature profile in the thickness direction.

2. Refined theories could be required for an accurate description of the stress and displacement field of both thick and thin plate geometries.

3. The models for the analysis of coupled thermo-mechanical problems permit to avoid the application of the Fourier's law because the temperature distribution through all the layers of the structure is automatically calculated.

References

[1] Librescu L., Marzocca P., Thermal stresses'03, vol.1, Virginia Polytechnic Institute and State University, 2003, Blacksburg, VA(USA).

[2] Librescu L., Marzocca P., Thermal stresses'03, vol.2, Virginia Polytechnic Institute and State University, 2003, Blacksburg, VA(USA).

[3] Noor A.K., Burton W.S., *Computational models for high-temperature multilayered composite plates and shells*, Applied Mechanics Reviews, 45(10), 419-446, 1992.

[4] Srinivas S., Rao A.K, *A Note on flexure of thick rectangular plates and laminates with variation of temperature across the thickness*, Bull Acad Pol Sci Ser Sci Tech, 20, 229-234, 1972.

[5] Bapu Rao M.N., *3D analysis of thermally loaded thick plates*, Nuclear Engineering and Design, 55, 353-361, 1979.

[6] Tungikar V.B., Rao K.M., *Three dimensional exact solution of thermal stresses in rectangular composite laminates*, Composite Structures, 27, 419-427, 1994.

[7] Bhaskar K., Varadan T.K., Ali J.S.M., *Thermoelastic solution for orthotropic and anisotropic composites laminates*, Composites Part B, 27B, 415-420, 1996.

[8] Carrera E., *A class of two-dimensional theories for anisotropic multilayered plates analysis*, Accademia delle Scienze di Torino, Memorie Scienze Fisiche, 19-20 (1995-1996), 1-39, 1995.

[9] Tauchert T.R., *Thermally induced flexure, buckling and vibration of plates*, Applied Mechanics Review, 44(8), 347-360, 1991.

[10] Noor A.K., Burton W.S., *Computational Models for high–temperature multilayered composite plates and shells*, Applied Mechanics Review, 45(10), 419-446, 1992.

[11] Argyris J., Tenek L., *Recent advances in computational thermo-structural analysis of composite plates and shells with strong nonlinearities*, Applied Mechanics Review, 50(5), 285-306, 1998.

[12] Librescu L., Elasto-statics and Kinetics of Anisotropic and Heterogeneous Shell-Type Structures, Noordhoff Int., Leyden, Netherland, 1975.

[13] Thornton E.A., Thermal Structures for Aerospace Applications, AIAA Educational Series, Reston, VA,1996.

[14] Reddy J.N., Mechanics of Laminated Composite Plates, Theory and Analysis. CRC Press, 1997.

[15] Carrera E., *An assessment of mixed and classical theories for the thermal stress analysis of orthotropic plate multilayerd plates*, Journal of Thermal Stress, 23, 797-831, 2000.

[16] Cho K.N., Bert C.W., Striz A.G., *Thermal Stress Analysis of Laminate Using Higher order Individual–Layer Theory* , Journal of Thermal Stress, 12, 321-332, 1989.

[17] Murakami H., *Assessment of Plate Theories for treating the thermo-mechanical response of layered plates*, Composite Engineering, 3(2), 137-149, 1993.

[18] Ali J.S.M., Bhaskar K., Varadan T.K., *A new theory for accurate thermal/mechanical flexural analysis of symmetric laminated plates*, Composite Structures, 45, 227-232, 1996.

[19] Zhou X., Chattopadhyay A., Gu H., *Dynamic response of smart composites using a coupled thermo-piezoelectric-mechanical model*, AIAA Journal, 38, 1939-1948, 2000.

[20] Gu H., Chattopadhyay A., Li J., Zhou X., *Higher order temperature theory for coupled thermo-piezoelectric-mechanical modeling of smart composites*, International Journal of Solids and Structures, 37, 6479-6497, 2000.

[21] Carrera E., *Temperature Profile Influence on Layered Plates Response Considering Classical and Advanced Theories*, AIAA Journal, 9, 1885-1896, 2002.

[22] Brischetto S., Carrera E., *Coupled thermo-mechanical analysis of one-layered and multilayered plates*, Applied Mechanics Reviews, 92(8), 1793-1812, 2010.

[23] Brischetto S., Carrera E., *Coupled thermo-mechanical analysis of one-layered and multilayered isotropic and composite shells*, Computer Modeling in Engineering and Sciences, 56(3), 249-301, 2010.

[24] Brischetto S., Leetsch R., Carrera E., Wallmersperger T., Kröplin B., *Thermo-mechanical bending of functionally graded plates*, Journal of Thermal Stresses, 31(3), 286-308, 2008.

[25] Brischetto S., Carrera E., *Thermal stress analysis by refined multilayered composite shell theories*, Journal of Thermal Stresses, 32(1), 165-186, 2009.

[26] Nowinski J.L., Theory of thermoelasticity with applications, Sijthoff and Noordoff, The Netherlands, 1978.

[27] Carrera E., Ciuffreda A., *Closed-form solutions to assess multilayered-plate theories for various thermal stress problems*, Journal of Thermal Stresses, 27, 1001-1031, 2004.

[28] Cinefra M., Carrera E., Brischetto S., Belouettar S., *Thermo-mechanical analysis of functionally graded shells*, Journal of Thermal Stresses, 33, 942-963, 2010.

[29] E. Carrera, *A class of two dimensional theories for multilayered plates analysis*, Atti Accademia delle Scienze di Torino, Mem. Sci. Fis., 19-20, 49-87, 1995.

[30] Fazzolari F.A., Carrera E., *Accurate free vibration analysis of thermo-mechanically pre/post-buckled anisotropic multilayered plates based on a refined hierarchical trigonometric Ritz formulation*, Composite Structures, 95, 381-402, 2013.

[31] Fazzolari F.A., Carrera E., *Free vibration analysis of sandwich plates with anisotropic face sheets in thermal environment by using the hierarchical trigonometric Ritz formulation*, Composites Part B: Engineering, page DOI:10.1016/j.compositesb.2013.01.020, 2013.

[32] Fazzolari F.A., Carrera E., *Thermo-mechanical buckling analysis of anisotropic multilayered composite and sandwich plates by using refined variable-kinematics theories*, Journal of Thermal Stresses, page DOI:10.1080/01495739.2013.770642, 2013.

[33] Robaldo A., Carrera E., Benjeddou A., *Unified Formulation for finite element thermoelastic analysis of multilayered anisotropic composite plates*, Journal of Thermal Stresses, 28, 1031-1065, 2005.

[34] Nali P., Carrera E., Calvi A., *Advanced fully-coupled thermo-mechanical plate elements for multilayered structures subjected to mechanical and thermal loading*, International Journal for Numerical Methods in Engineering, 85, 896-919, 2011.

[35] Murakami H., *Laminated composite plate theory with improved in-plane response*, Journal of Applied Mechanics, vol 53, pp 661-666, 1986.

[36] Reissner E., *On a certain mixed variational theory and a proposed applications*, International Journal of Numerical Methods in Engineering, 20, 1366-1368, 1984.

[37] Carrera E., *Developments, Ideas and Evaluations based upon the Reissner's Mixed Variational Theorem in the Modeling of Multilayered Plates and Shells*, Applied Mechanics Review, 54, 301-329, 2001.

[38] Brischetto S., Carrera E., *Heat conduction and thermal analysis in multilayered plates and shells*, Mechanics Research Communications, 38, 449-455, 2011.

[39] Carrera E., *Developments, ideas and evaluations based upon Reissner's Mixed Variational Theorem in the modeling of multilayered plates and shells*, Applied Mechanics Reviews, 54, 301-329, 2001.

[40] Khare R.K., Kant T., Garg A.K., *Closed-form thermo-mechanical solutions of higher-order theories of cross-ply laminated shallow shells*, Composite Structures, 59(3), 313-340, 2003.

[41] Khdeir A.A., Rajab M.D., Reddy J.N., *Thermal effects on the response of cross-ply laminated shallow shells*, International Journal of Solids and Structures, 29(5), 653-667, 1992.

[42] Fazzolari F.A., Carrera E., *Advanced variable kinematics Ritz and Galerkin formulation for accurate buckling and vibration analysis of laminated composite plates*, Composite Structures, 94(1), 50-67, 2011.

[43] Fazzolari F.A., Carrera E., *Advances in the Ritz formulation for free vibration response of doubly-curved anisotropic laminated composite shallow and deep shells*, Composite Structures, page DOI:10.1016/j.compstruct.2013.01.018, 2013.

[44] Carrera E., Fazzolari F.A., Demasi L., *Vibration analysis of anisotropic simply supported plates by using variable kinematic and Rayleigh-Ritz method*, Journal of Vibration and Acoustics, 133(6), 061017-1/061017-16, 2011.

[45] Bhaskar K., Varadan T.K., Ali J.S.M., *Thermoelastic Solution for Orthotropic and Anisotropic Composites Laminates*, Composite Part B , 27, 415-420, 1986.

[46] Ali J.S.M., Bhaskar K., Varadan T.K., *A new theory for accurate thermal/mechanical flexural analysis of symmetric laminated plates*, Composite Structures, 45, 227-232, 1999.

Table 1: Transverse displacement and transverse shear stress of thick and thin plates. Comparison of different theories to exact solutions.

	$\bar{U}_z$ at $z = \mp h/2$		S_{xz} at $z = \mp h/6$	
a/h	4	100	4	100
Exact	42.69	10.26	84.81	7.073
Layer-Wise Theories				
	RMVT Applications			
LM4	42.69	10.26	84.81	7.073
LM3	42.70	10.26	84.85	7.073
LM2	42.74	10.26	84.90	7.073
LM1	42.62	10.33	94.74	7.498
	PVD Applications no IC			
LD4	42.69	10.26	84.81	7.073
LD3	42.68	10.26	84.82	7.073
LD2	42.25	10.26	82.92	7.073
LD1	41.24	10.92	235.4	7.672
Equivalent Single Layer Theories				
	RMVT Applications			
			Including ZZ and IC	
EMZC3	42.44	10.26	83.81	7.073
EMZC2	41.99	10.26	89.04	7.074
EMZC1	36.96	16.12	116.3	9.198
			Including IC	
EMC4	42.18	10.25	96.37	7.076
EMC3	42.26	10.25	96.15	7.076
EMC2	34.76	10.23	120.16	7.079
EMC1	30.64	16.09	150.39	9.205
	PVD Applications			
			Including ZZ	
EDZ3	42.34	10.26	96.4	7.076
EDZ2	17.00	10.26	102.72	7.077
EDZ1	36.61	16.12	137.04	9.203
			Discarding IC and ZZ	
ED4	42.05	10.25	88.64	7.075
ED3	42.04	10.25	88.62	7.075
ED2	34.74	10.23	116.2	7.079
ED1	30.42	16.09	144.2	9.204
FSDT	30.42	16.09	151.8	9.206
CLT	10.18	10.18	177.1	7.089

Table 2: Influence of thickness ratio to transverse displacement $\bar{U}_z$. Comparison between assumed and calculated temperature profiles. for advanced mixed theories formulated on the basis of RMVT.

		a/h			
Theory	$T(z)$	2	4	10	100
RMVT Applications					
3D	T_a	96.79	42.69	17.39	10.26
	T_c	-	-	-	-
	Layer-Wise Theories (`no IC`)				
LM4	T_a	96.79	42.69	17.39	10.26
	T_c	75.60	37.91	16.92	10.26
LM3	T_a	96.77	42.68	17.39	10.26
	T_c	104.77	43.06	15.86	8.53
LM2	T_a	95.74	42.55	17.39	10.26
	T_c	109.43	56.29	25.15	14.64
LM1	T_a	96.86	42.62	17.36	10.33
	T_c	81.31	38.90	16.96	10.33
	Equivalent Single Layer Theories				
			`Including ZZ and IC`		
EMZC3	T_a	95.26	42.42	17.38	10.26
	T_c	40.83	30.52	15.53	10.24
EMZC2	T_a	93.74	41.44	17.04	10.26
	T_c	3.79	15.74	18.55	16.09
EMZC1	T_a	50.82	36.65	21.63	16.16
	T_c	37.88	15.74	18.55	16.09
			`Theories including IC`		
EMC4	T_a	98.26	42.18	16.96	10.25
	T_c	40.70	30.34	15.17	10.24
EMC3	T_a	98.16	42.26	17.00	10.25
	T_c	25.82	29.50	16.01	10.25
EMC2	T_a	83.12	34.76	14.98	10.23
	T_c	6.19	14.93	12.85	10.22
EMC1	T_a	42.29	30.64	19.61	16.09
	T_c	3.15	13.16	16.81	16.08

Table 3: Influence of thickness ratio to transverse displacement $\bar{U}_z$. Comparison between assumed and calculated temperature profiles. for classical theories formulated on the basis of PVD.

		a/h			
Theory	$T(z)$	2	4	10	100
3D	T_a	96.79	42.69	17.39	10.26
	T_c	-	-	-	-
PVD Applications					
	Layer-Wise Theories				
LD4	T_a	96.78	42.69	17.39	10.26
	T_c	75.16	37.91	16.92	10.26
LD3	T_a	96.73	42.68	17.39	10.26
	T_c	104.76	43.06	15.86	8.53
LD2	T_a	94.34	42.25	17.36	10.26
	T_c	108.37	55.88	25.09	14.64
LD1	T_a	89.25	41.24	17.92	10.91
	T_c	73.73	37.30	17.19	10.91
	Equivalent Single Layer Theories				
				`Including ZZ`	
EDZ3	T_a	94.87	42.34	17.37	10.26
	T_c	40.82	30.49	15.52	10.24
EDZ2	T_a	93.26	41.34	17.00	10.26
	T_c	6.95	17.76	14.58	10.24
EDZ1	T_a	50.06	36.61	21.61	16.12
	T_c	3.73	15.72	18.53	16.09
				`Discarding ZZ and IC`	
ED4	T_a	98.22	42.05	16.90	10.25
	T_c	40.73	30.29	15.12	10.24
ED3	T_a	98.15	42.04	16.90	10.25
	T_c	25.79	29.33	15.91	10.24
ED2	T_a	83.47	34.74	14.96	10.23
	T_c	6.22	14.92	12.83	10.21
ED1	T_a	42.71	30.42	19.45	16.09
	T_c	3.18	13.06	16.68	16.07
FSDT	T_a	43.97	30.37	19.30	16.09
	T_c	3.27	13.04	16.55	16.07
CLT	T_a	16.05	16.05	16.05	16.05
	T_c	1.196	6.895	13.77	16.03

Table 4: Cylindrical shell: geometry and materials properties.

$E_1/E_2[-]$	25
$E_2 = E_3[-]$	–
$G_{12}/G_{23}[-]$	2.5
$G_{12} = G_{13}[-]$	–
$\nu_{12} = \nu_{13} = \nu_{23}[-]$	0.25
$\alpha_{22}/\alpha_{11}[-]$	3
$\alpha_{11} = \alpha_{12} = \alpha_{33}[-]$	–
$\alpha_{11} = \alpha_{13} = \alpha_{23}[-]$	–
$a = b[m]$	1
$h[m]$	0.1
$h_{0^\circ} = h_{90^\circ}[m]$	0.05
$R_\alpha[m]$	∞
$R_\beta[m]$	5,10,50

Table 5: Spherical shell: geometry and materials properties.

faces	
$E_1[10^6 psi]$	25
$E_2 = E_3[10^6 psi]$	1
$G_{12} = G_{13}[10^6 psi]$	0.5
$G_{23}[10^6 psi]$	0.2
$\nu_{12} = \nu_{13} = \nu_{23}[-]$	0.25
$\alpha_{22}[10^{-5}/^\circ C]$	2
$\alpha_{11} = \alpha_{33}[10^{-5}/^\circ C]$	0.1
$\alpha_{12} = \alpha_{13} = \alpha_{23}[10^{-5}/^\circ C]$	0.1
core	
$E_1 = E_2[10^6 psi]$	0.04
$E_3[10^6 psi]$	0.5
$G_{12}[10^6 psi]$	0.016
$G_{13} = G_{23}[10^6 psi]$	0.06
$\nu_{12} = \nu_{13} = \nu_{23}[-]$	0.02
$\alpha_{22}[10^{-5}/^\circ C]$	0.2
$\alpha_{11} = \alpha_{33}[10^{-6}/^\circ C]$	0.1
$\alpha_{12} = \alpha_{13} = \alpha_{23}[10^{-6}/^\circ C]$	0.1
geometry	
$a = b[m]$	1
$h[m]$	0.25, 0.01
$h_c[m]$	$0.8h$
$h_f(0^\circ/c/0^\circ)[m]$	$0.1h$
$h_f(0^\circ/90^\circ/c/90^\circ/0^\circ)[m]$	$0.05h$
$R_\alpha = R_\beta[m]$	5,10,20

Table 6: Linear through the thickness thermal load. Cylindrical shell ($0^\circ/90^\circ$) with thickness ratio $a/h = 10$. Equivalent Single Layer theories. Transverse displacement $\bar{u}_z = \frac{u_z(a/2,b/2,0)}{\alpha_1 T_1 b^2}$.

R/a	5	10	50
HOST12[40]	1.1261	1.1434	1.1493
HSDT[41]	1.1235	1.1421	1.1482
	ESL theories		
CLT	1.1834	1.1966	1.1997
FSDT	1.1805	1.1959	1.1997
ED1	1.1806	1.1959	1.1997
ED2	1.1255	1.1411	1.1455
ED3	1.1264	1.1422	1.1466
ED4	1.1276	1.1434	1.1479
	Zig-Zag theories		
EDZ1	1.1203	1.1361	1.1406
EDZ2	1.1260	1.1416	1.1460
EDZ3	1.1259	1.1416	1.1460

Table 7: Linear through the thickness thermal load. Cylindrical shell ($0°/90°$) with thickness ratio $a/h = 10$. Layer Wise theories. Transverse displacement $\bar{u}_z = \frac{u_z(a/2,b/2,0)}{\alpha_1 T_1 b^2}$.

R/a	5	10	50
ED4	1.1276	1.1434	1.1479
LW theories			
LD1	1.1425	1.1577	1.1620
LD2	1.1262	1.1414	1.1457
LD3	1.1280	1.1434	1.1477
LD4	1.1280	1.1434	1.1477

Table 8: Linear through the thickness thermal load. Spherical shell ($0°/core/0°$) with thickness ratio $a/h = 4$ and $a/h = 100$. Equivalent Single Layer theories. Transverse displacement $\bar{u}_z = \frac{10hu_z(a/2,b/2,0)}{\alpha_1 T_1 a^2}$.

R/a	5	10	20	plate	5	10	20	plate
	$a/h = 4$				$a/h = 100$			
HOST12[40]	4.2032	4.2343	4.2422	4.2448	0.8780	1.4368	1.7077	1.8221
FOST[40]	3.2618	3.2745	3.2775	3.2784	0.8624	1.4085	1.6726	1.7840
ESL theories								
CLT	1.8043	1.8025	1.8021	1.8019	0.8750	1.4256	1.6904	1.8019
FSDT	3.1472	3.1632	3.1672	3.1685	0.8738	1.4264	1.6931	1.8055
ED1	3.1466	3.1631	3.1672	3.1685	0.8781	1.4293	1.6941	1.8055
ED2	3.0306	3.0471	3.0512	3.0525	0.8764	1.4343	1.7045	1.8185
ED3	4.1867	4.2308	4.2419	4.2456	0.8789	1.4383	1.7092	1.8235
ED4	4.1928	4.2360	4.2469	4.2505	0.8658	1.4178	1.6853	1.7983
Zig-Zag theories								
EDZ1	4.3705	4.4190	4.4312	4.4352	0.8822	1.4347	1.6997	1.8112
EDZ2	4.3228	4.3720	4.3843	4.3885	0.8800	1.4395	1.7102	1.8244
EDZ3	4.3261	4.3754	4.3878	4.3919	0.8800	1.4395	1.7102	1.8244

Table 9: Linear through the thickness thermal load. Spherical shell ($0°/core/0°$) with thickness ratio $a/h = 4$ and $a/h = 100$. Layer Wise theories. Transverse displacement $\bar{u}_z = \frac{10hu_z(a/2,b/2,0)}{\alpha_1 T_1 a^2}$.

R/a	5	10	20	plate	5	10	20	plate
	$a/h = 4$				$a/h = 100$			
ED4	4.1928	4.2360	4.2469	4.2505	0.8658	1.4178	1.6853	1.7983
LW theories								
LD1	4.3417	4.3653	4.3712	4.3732	0.8640	1.4122	1.6779	1.7901
LD2	4.3420	4.3651	4.3709	4.3729	0.8637	1.4118	1.6774	1.7896
LD3	4.3427	4.3658	4.3716	4.3736	0.8637	1.4118	1.6774	1.7896
LD4	4.3426	4.3657	4.3715	4.3735	0.8637	1.4118	1.6774	1.7896

Table 10: Linear through the thickness thermal load. Spherical shell $(0°/90°/core/90°/0°)$ with thickness ratio $a/h = 4$. Equivalent Single Layer theories. Transverse displacement $\bar{u}_z = \frac{10hu_z(a/2,b/2,0)}{\alpha_1 T_1 a^2}$.

R/a	5	10	20	plate
HOST12[40]	1.7738	1.7915	1.7959	1.7974
FOST[40]	1.7771	1.7768	1.7893	1.7901
		ESL theories		
CLT	1.8031	1.8022	1.8020	1.8019
FSDT	1.7988	1.8087	1.8111	1.8120
ED1	1.7984	1.8086	1.8111	1.8120
ED2	1.6523	1.6624	1.6649	1.6658
ED3	1.7700	1.7902	1.7952	1.7969
ED4	1.8125	1.8321	1.8370	1.8386
		Zig-Zag theories		
EDZ1	1.7976	1.8091	1.8120	1.8129
EDZ2	1.6602	1.6718	1.6747	1.6756
EDZ3	1.7642	1.7845	1.7897	1.7914

Table 11: Linear through the thickness thermal load. Spherical shell $(0°/90°/core/90°/0°)$ with thickness ratio $a/h = 4$. Layer Wise theories. Transverse displacement $\bar{u}_z = \frac{10hu_z(a/2,b/2,0)}{\alpha_1 T_1 a^2}$.

R/a	5	10	20	plate
ED4	1.8125	1.8321	1.8370	1.8386
		LW theories		
LD1	1.8046	1.8206	1.8246	1.8260
LD2	1.8060	1.8220	1.8260	1.8273
LD3	1.8059	1.8219	1.8260	1.8273
LD4	1.8059	1.8219	1.8259	1.8273

Table 12: Angle-ply composite plates

MAT-1									
E_1 [GPa]	E_2, E_3 [GPa]	G_{12}, G_{13} [GPa]	G_{23} [GPa]	ν_{12}, ν_{13} [−]	ν_{23} [−]	α_1 [1/K]	α_2 [1/K]	C_v [J/Kg/K]	ρ [Kg/m^3]
127.6	11.3	6.0	1.8	0.30	0.36	−0.9 E-6	27.0 E-6	921	1633.1
MAT-2									
E_1 [GPa]	E_2, E_3 [GPa]	G_{12}, G_{13} [GPa]	G_{23} [GPa]	ν_{12}, ν_{13} [−]	ν_{23} [−]	α_1 [1/K]	α_2 [1/K]	C_v [J/Kg/K]	ρ [Kg/m^3]
76	5.5	2.3	0.8	0.34	0.34	−5.32 E-6	42.4 E-6	1800	1550.1
MAT-3									
E_1/E_2	G_{12}/E_2	G_{13}/E_2	G_{23}/E_2	ν_{12}	α_1/α_0	α_2/α_0	α_0 [1/K]		
40	0.6	0.6	0.5	0.25	0.02	22.5	1.0 E-6		

Table 13: Sandwich plate with laminated angle-ply face sheets

MAT-4			
Face Sheets			
E_1/E_2	G_{12}/E_2	G_{23}/E_2	ν_{12}
19.0	0.52	0.338	0.32
ν_{13}	ν_{23}	α_1/α_0	α_2/α_0
0.32	0.49	0.001	1.0
Core			
E_1/E_2^f	E_2/E_2^f	E_3/E_2^f	G_{12}/E_2^f
3.2×10^{-5}	2.9×10^{-5}	0.4	2.4×10^{-3}
G_{13}/E_2^f	G_{23}/E_2^f	ν_{12}	ν_{13}
7.9×10^{-2}	6.6×10^{-2}	0.99	3.0×10^{-5}
ν_{23}	α_1/α_0	α_2/α_0	$\rho_c/\rho^{f(1)}$
3.0×10^{-5}	1.36	1.36	0.07

Table 14: Convergence analysis of the critical temperature variation ΔT_{cr} [K] for angle-ply laminate by using ED_{222} theory.

M, N	RM	GM	GGM	RM	GM	GGM	RM	GM	GGM
	$[15^\circ/-15^\circ]_s$			$[22.5^\circ/-22.5^\circ]_s$			$[30^\circ/-30^\circ]_s$		
2	168.562	165.408	168.544	233.463	224.388	233.420	264.991	274.924	265.075
4	158.949	158.262	159.970	212.329	207.434	213.501	253.400	264.517	254.016
6	157.585	157.419	158.909	209.335	205.275	211.116	249.699	262.133	250.985
8	156.981	157.105	158.503	207.963	204.431	210.173	247.766	261.144	249.583
10	156.629	156.941	158.283	207.150	203.987	209.655	246.545	260.616	248.752
12	156.394	156.842	158.140	206.605	203.715	209.317	245.693	260.294	248.186
	$[45^\circ/-45^\circ]_s$			$[67.5^\circ/-67.5^\circ]_s$			$[75^\circ/-75^\circ]_s$		
2	290.789	302.644	290.884	233.463	224.388	233.420	168.562	165.408	168.544
4	277.057	290.953	277.608	212.329	207.434	213.501	158.949	158.262	159.970
6	272.011	287.667	273.591	209.335	205.275	211.116	157.585	157.419	158.909
8	269.271	286.251	271.737	207.963	204.431	210.173	156.981	157.105	158.503
10	267.499	285.483	270.655	207.150	203.987	209.655	156.629	156.941	158.283
12	266.242	285.010	269.932	206.605	203.715	209.317	156.394	156.842	158.140

Table 15: Pure thermal and pure mechanical buckling loads

	Theory	θ				
		0.00	22.5	45	67.5	90
ΔT [K]	ED_{111}	130.872	222.405	277.222	222.405	130.872
	ED_{222}	118.128	206.605	266.242	206.605	118.128
	ED_{444}	117.888	205.835	265.651	205.835	117.888
	LD_{222}	117.906	205.625	265.294	205.625	117.906
σ_{xx} [MPa]	ED_{111}	58.379	67.205	77.859	58.530	39.078
	ED_{222}	55.757	64.283	74.758	54.373	35.274
	ED_{444}	55.681	64.206	74.551	54.148	35.205
	LD_{222}	55.681	64.124	74.489	54.114	35.207
σ_{xx}, σ_{yy} [MPa]	ED_{111}	29.189	33.547	38.960	33.547	29.189
	ED_{222}	27.879	32.070	37.413	32.070	27.879
	ED_{444}	27.840	32.009	37.328	32.009	27.840
	LD_{222}	27.840	31.991	37.280	31.991	27.840
σ_{xy} [MPa]	ED_{111}	124.821	96.768	104.208	96.768	124.821
	ED_{222}	115.600	90.375	98.231	90.375	115.600
	ED_{444}	115.055	89.963	97.909	89.963	115.055
	LD_{222}	115.054	89.859	97.530	89.859	115.054
$\sigma_{xx}, \sigma_{yy}, \sigma_{xy}$ [MPa]	ED_{111}	27.879	37.020	44.403	37.020	27.879
	ED_{222}	26.593	35.634	42.942	35.634	26.593
	ED_{444}	26.535	35.539	42.783	35.539	26.535
	LD_{222}	26.535	35.513	42.726	35.513	26.535

Table 16: Convergence analysis Q9 element

LD4 Q9 S=4					
N_e	2×2	4×4	6×6	10×10	Exact [45]
$\bar{u}(0,\frac{b}{2},\mp\frac{h}{2})$	± 18.74	± 18.17	± 18.12	± 18.11	± 18.11
$\bar{v}(\frac{a}{2},0,\mp\frac{h}{2})$	± 84.06	± 82.02	± 81.90	± 81.85	± 81.83
$\bar{w}(\frac{a}{2},\frac{b}{2},\pm\frac{h}{2})$	43.41	42.72	42.68	42.68	42.69

Table 17: Assumed temperature profile. Out of plane displacement $\bar{w}(\frac{a}{2},\frac{b}{2},\mp\frac{h}{2})$ results. Errors measured with regards to [45].

$\bar{w}(\frac{a}{2},\frac{b}{2},\pm\frac{h}{2})$ Q9 $[6\times 6]$								
S	4		10		20		100	
Exact [45]	42.69		17.39		12.12		10.26	
Ali et al. [46]	42.34		17.37		12.12			
LD 1	41.25	(−3.37%)	17.63	(1.37%)	12.67	(4.50%)	10.92	(6.38%)
LM 1	42.63	(−0.16%)	17.36	(−0.16%)	12.17	(0.42%)	10.34	(0.71%)
LD 2	42.26	(−1.01%)	17.37	(−0.10%)	12.12	(−0.01%)	10.26	(0.00%)
LM 2	42.57	(−0.30%)	17.39	(−0.02%)	12.12	(0.00%)	10.26	(0.00%)
LD 3	42.69	(0.00%)	17.40	(0.03%)	12.12	(0.02%)	10.26	(0.00%)
LM 3	42.69	(0.00%)	17.39	(0.00%)	12.12	(0.01%)	10.26	(0.00%)
LD 4	42.69	(0.00%)	17.40	(0.03%)	12.12	(0.02%)	10.26	(0.00%)
LM 4	42.70	(0.01%)	17.39	(0.00%)	12.12	(0.01%)	10.26	(0.00%)
ED 1	30.43	(−28.7%)	19.46	(11.8%)	16.97	(40.0%)	16.10	(56.8%)
EM 1	30.66	(−28.1%)	19.60	(12.7%)	17.02	(40.3%)	16.10	(56.8%)
ED 2	34.74	(−18.6%)	14.96	(−13.9%)	11.43	(−5.75%)	10.23	(−0.28%)
EM 2	34.76	(−18.5%)	14.99	(−13.8%)	11.43	(−5.68%)	10.23	(−0.28%)
ED 3	42.05	(−1.50%)	16.91	(−2.79%)	11.97	(−1.29%)	10.26	(−0.07%)
EM 3	42.28	(−0.98%)	17.00	(−2.23%)	12.00	(−1.04%)	10.26	(−0.05%)
ED 4	42.06	(−1.49%)	16.91	(−2.79%)	11.97	(−1.29%)	10.26	(−0.07%)
EM 4	42.20	(−1.16%)	16.96	(−2.48%)	11.98	(−1.15%)	10.26	(−0.06%)
EDZ1	36.62	(−14.2%)	21.62	(24.2%)	17.60	(45.20%)	16.12	(57.1%)
EMZ1	36.68	(−14.0%)	21.63	(24.3%)	17.61	(45.25%)	16.12	(57.1%)
EDZ2	41.35	(−3.15%)	17.01	(−2.19%)	12.01	(−0.91%)	10.26	(−0.04%)
EMZ2	41.46	(−2.90%)	17.04	(−2.03%)	12.02	(−0.83%)	10.26	(−0.04%)
EDZ3	42.34	(−0.82%)	17.38	(−0.07%)	12.12	(−0.01%)	10.26	(0.00%)
EMZ3	42.42	(−0.63%)	17.38	(−0.08%)	12.12	(−0.02%)	10.26	(0.00%)

Table 18: Calculated temperature profile. Out of plane displacement $\bar{w}(\frac{a}{2}, \frac{b}{2}, \mp\frac{h}{2})$ results.

$\bar{w}(\frac{a}{2}, \frac{b}{2}, \pm\frac{h}{2})$ Q9 $[6 \times 6]$				
S	4	10	20	100
Exact [45]	42.69	17.39	12.12	10.26
Ali et al. [46]	42.34	17.37	12.12	
LD 1	37.28	17.19	12.57	10.91
LM 1	38.88	16.95	12.09	10.33
LD 2	32.10	16.39	11.93	10.25
LM 2	32.29	16.40	11.93	10.25
LD 3	32.18	16.40	11.93	10.25
LM 3	32.18	16.39	11.93	10.25
LD 4	32.12	16.40	11.93	10.25
LM 4	32.12	16.39	11.93	10.25
ED 1	27.00	18.90	16.84	16.09
EM 1	27.21	19.04	16.88	16.09
ED 2	26.11	14.10	11.24	10.22
EM 2	26.12	14.12	11.25	10.22
ED 3	32.06	15.95	11.78	10.24
EM 3	32.25	16.04	11.81	10.25
ED 4	31.57	15.93	11.78	10.24
EM 4	31.68	15.98	11.79	10.25
EDZ1	28.30	20.41	17.33	16.11
EMZ1	28.41	20.42	17.33	16.11
EDZ2	31.62	16.06	11.82	10.25
EMZ2	31.75	16.09	11.83	10.25
EDZ3	32.43	16.41	11.93	10.25
EMZ3	32.49	16.41	11.93	10.25

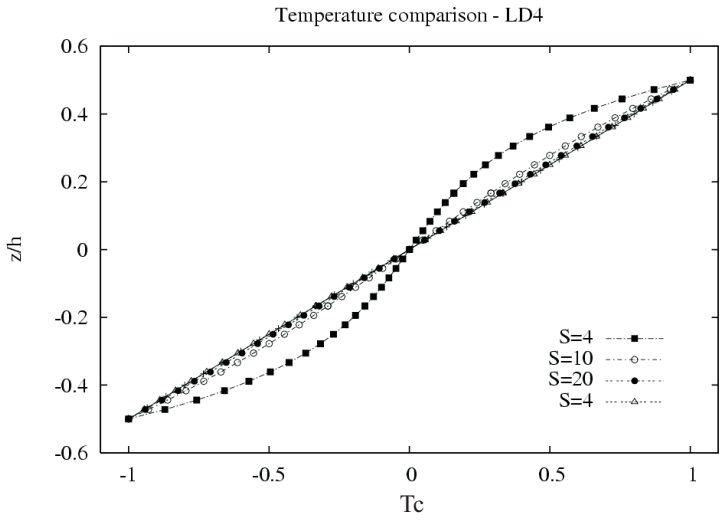

Figure 1: Calculated temperature profile for various thickness parameters.

Figures

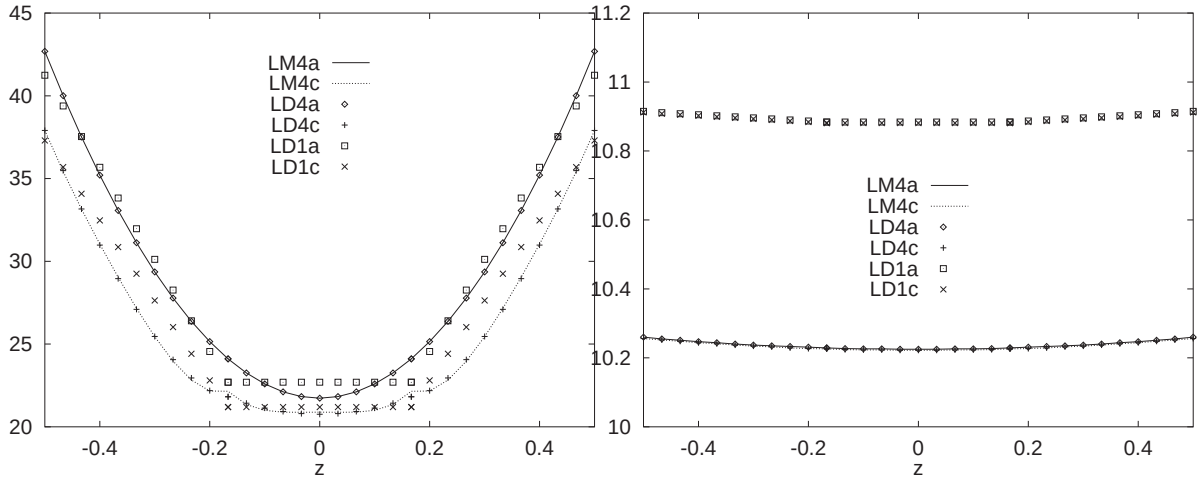

a) Layer-Wise $a/h = 4$ *b) Layer-Wise $a/h = 100$*

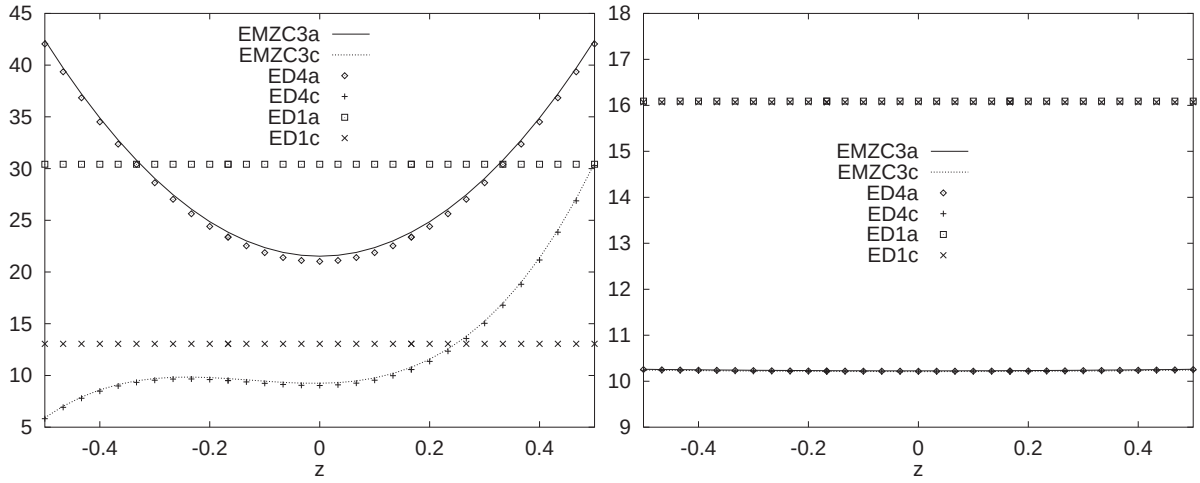

c) Equivalent Single Layer $a/h = 4$ *d) Equivalent Single Layer $a/h = 100$*

Figure 2: Plate results. Transverse displacement $\bar{U}_z(a/2, b/2)$ distribution vs z. Comparison of various theories in the two cases of assumed and calculated temperature profiles.

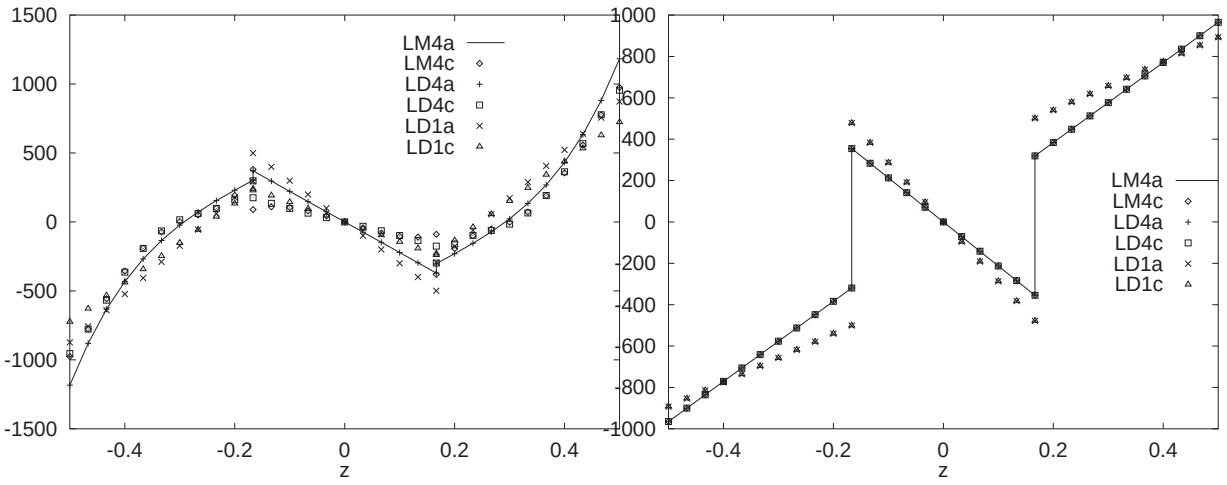

a) Layer-Wise $a/h = 4$ *b) Layer-Wise $a/h = 100$*

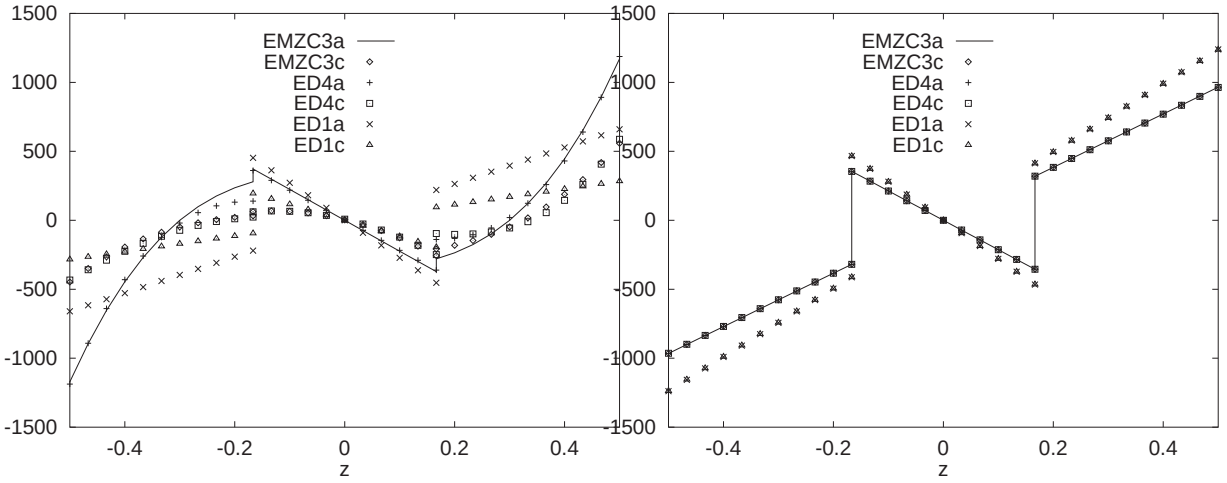

c) Equivalent Single Layer $a/h = 4$ *d) Equivalent Single Layer $a/h = 100$*

Figure 3: Plate results. In-plane normal stress $\bar{S}_{xx}(a/2, b/2)$ distribution vs z. Comparison of various theories in the two cases of assumed and calculated temperature profiles.

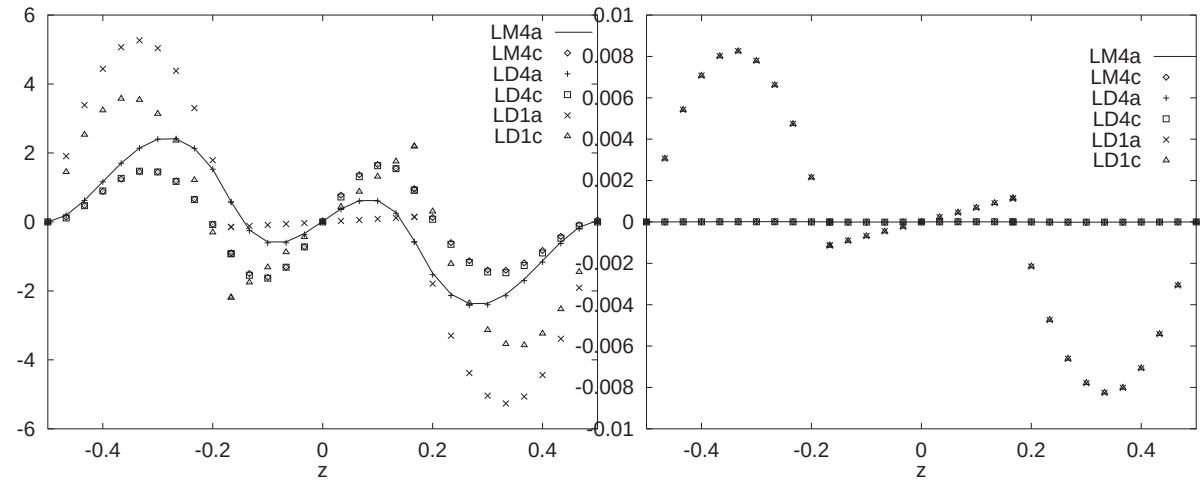

a) Layer-Wise $a/h = 4$ *b) Layer-Wise $a/h = 100$*

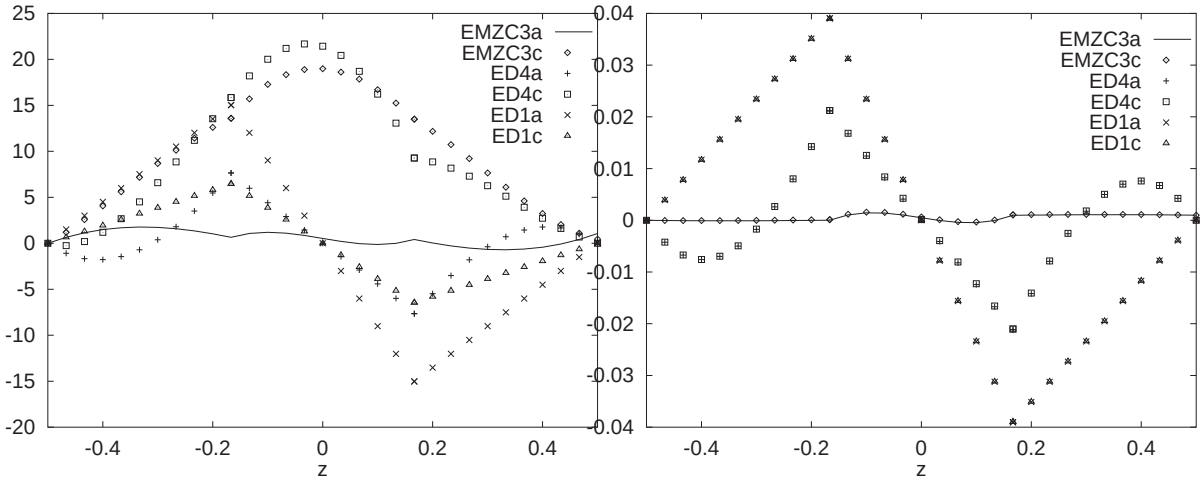

c) Equivalent Single Layer $a/h = 4$ *d) Equivalent Single Layer $a/h = 100$*

Figure 4: Plate results. Out-of-plane normal stress $\bar{S}_{zz}(a/2, b/2)$ distribution vs z. Comparison of various theories in the two cases of assumed and calculated temperature profiles.

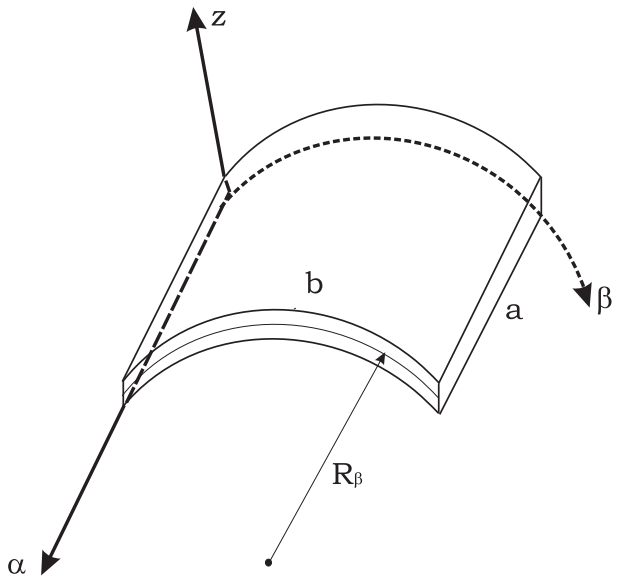

Figure 5: Geometry and notations for a cylindrical shell, particular case of spherical shell when $R_\alpha = \infty$.

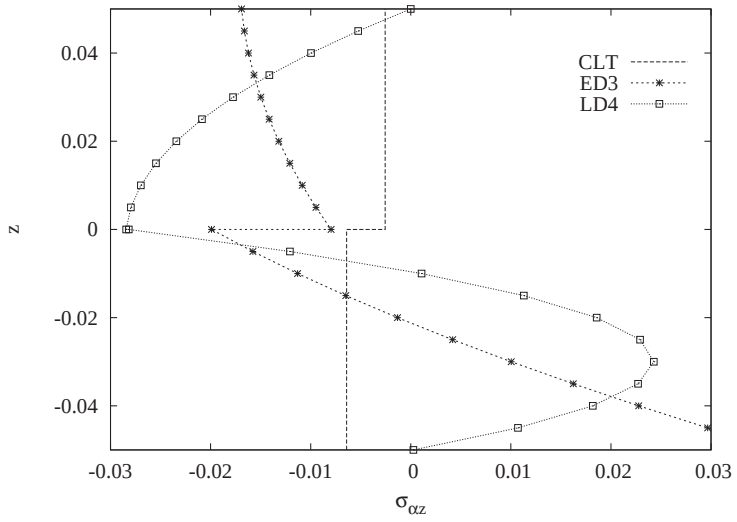

Figure 6: Cylindrical shell (0°/90°) with radius of curvature $R_\beta/a = 10$. Transverse shear stress $\sigma_{\alpha z}$ through the thickness z. Thickness ratio $a/h = 10$.

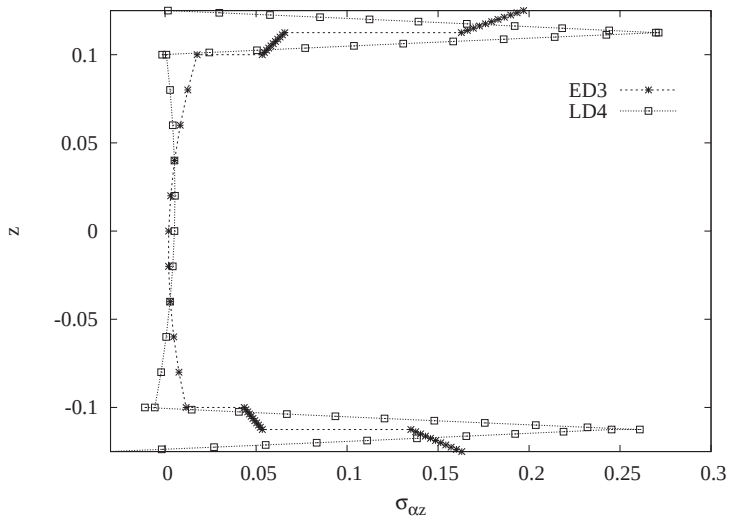

Figure 7: Spherical shell $(0°/90°/core/90°/0°)$ with radius of curvature $R_\beta/a = 10$. Transverse shear stress $\sigma_{\alpha z}$ through the thickness z. Thickness ratio $a/h = 4$.

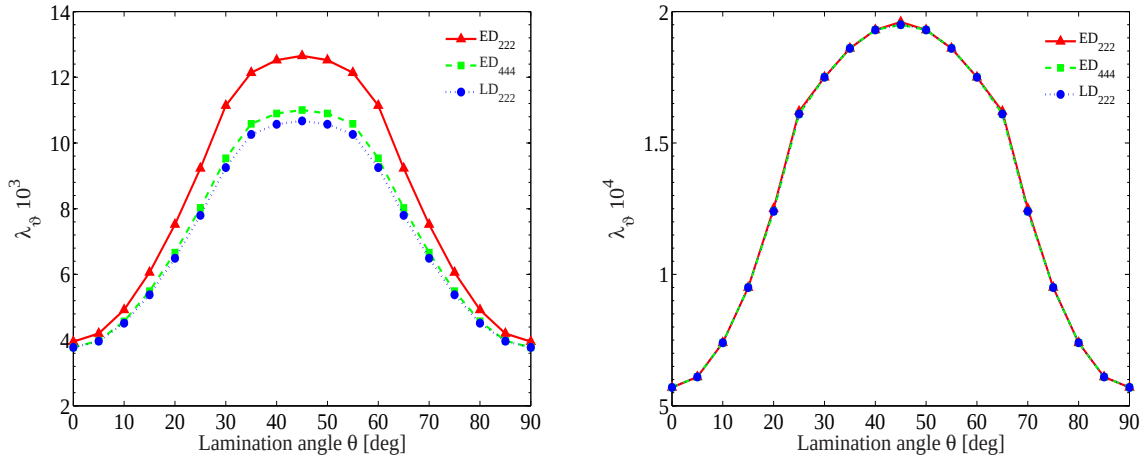

(a) $a/h = 10$ (b) $a/h = 100$

Figure 8: Critical temperature parameter $\lambda_\vartheta = \alpha_0 \, \mathrm{T}_{cr}$, varying the lamination angle and the plate theory, $\frac{a}{b} = 1$.

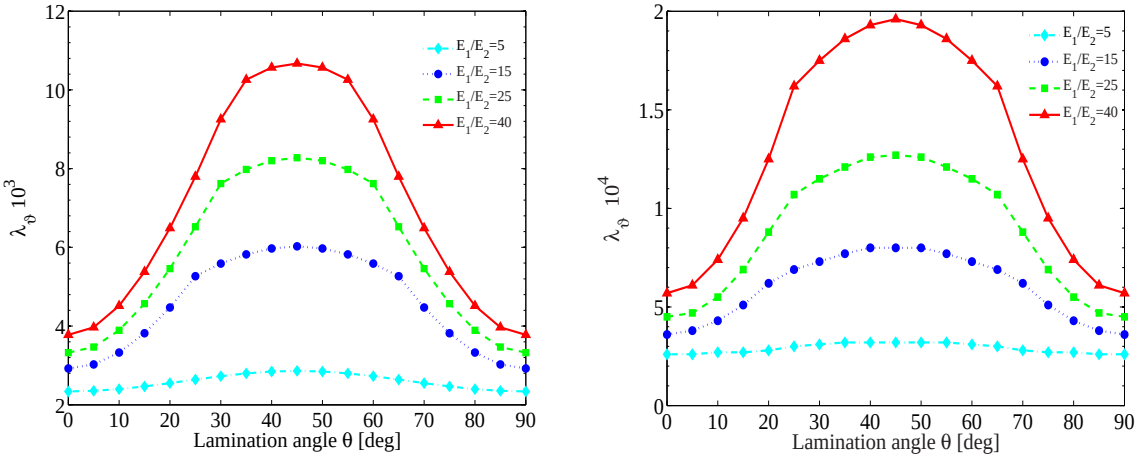

(a) $a/h = 10$ (b) $a/h = 100$

Figure 9: Critical temperature parameter $\lambda_\vartheta = \alpha_0\, \mathrm{T}_{cr}$, varying θ and $\mathrm{E}_1/\mathrm{E}_2$, $\frac{a}{b} = 1$.

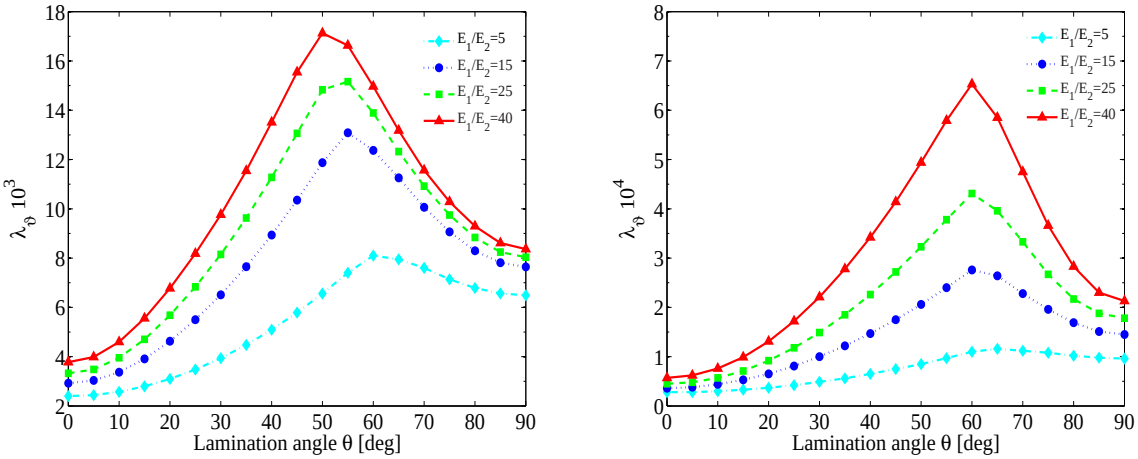

(a) $a/h = 10$ (b) $a/h = 100$

Figure 10: Critical temperature parameter $\lambda_\vartheta = \alpha_0\, \mathrm{T}_{cr}$, varying θ and $\mathrm{E}_1/\mathrm{E}_2$, $\frac{a}{b} = 2$.

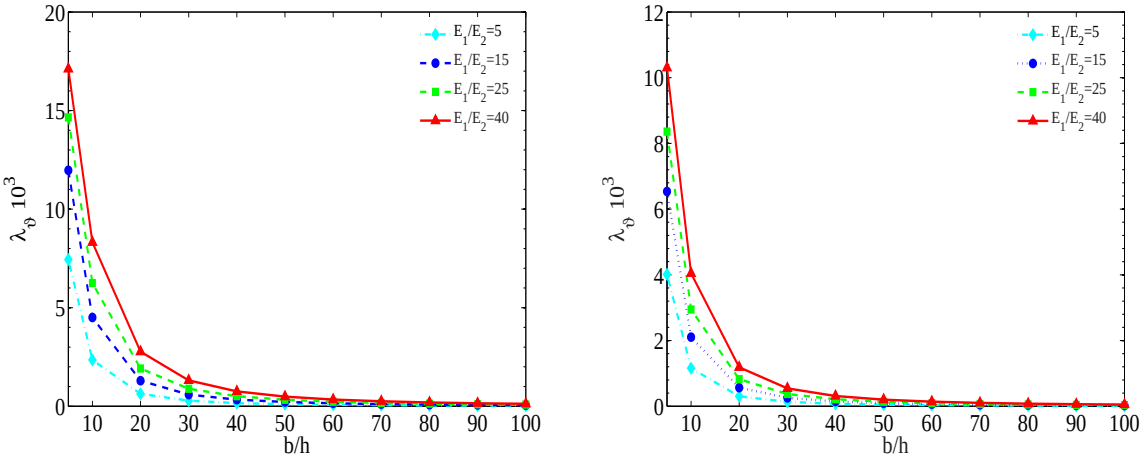

(a) $a/b = 1$ (b) $a/b = 2$

Figure 11: Critical temperature parameter $\lambda_\vartheta = \alpha_0\, \mathrm{T}_{cr}$, varying the b/h and $\mathrm{E}_1/\mathrm{E}_2$, symmetric cross ply laminate.

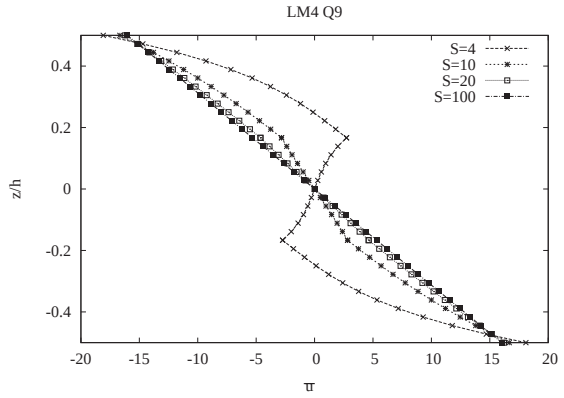

(a) $\bar{u}(0.0, \frac{b}{2})$ LM4

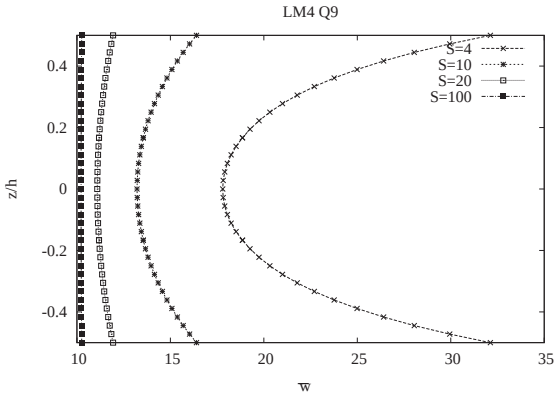

(b) $\bar{w}(\frac{a}{2}, \frac{b}{2})$ LM4

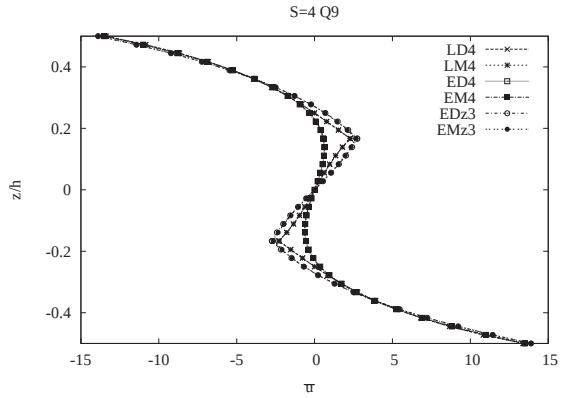

(c) $\bar{u}(\frac{a}{2}, \frac{b}{2})$ S=4

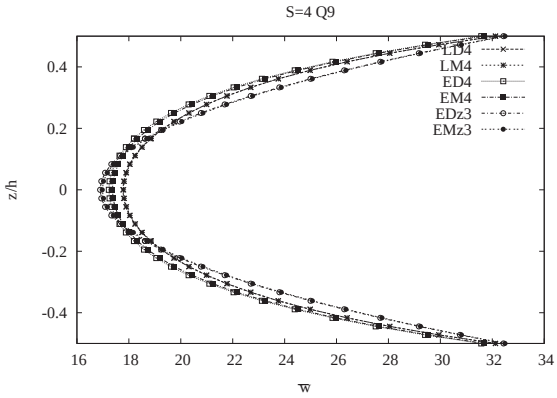

(d) $\bar{w}(\frac{a}{2}, \frac{b}{2})$ S=4

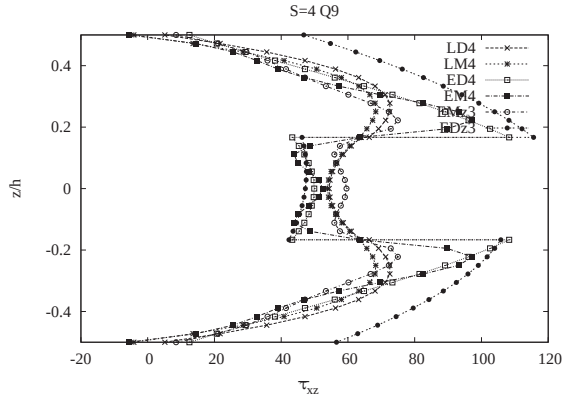

(e) $\sigma^{-}_{xz}(0.0, \frac{b}{2})$ S=4

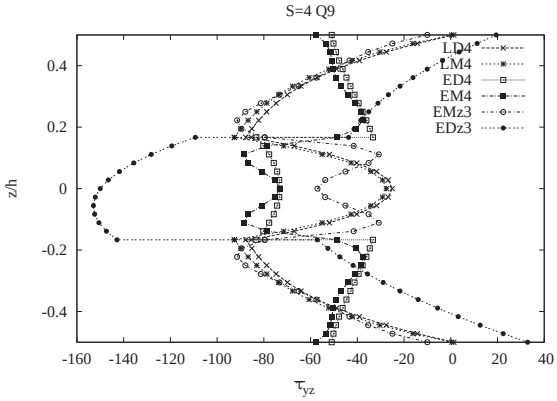

(f) $\sigma^{-}_{yz}(\frac{a}{2}, 0.0)$ S=4

Figure 12: Various results for the actual temperature profile.

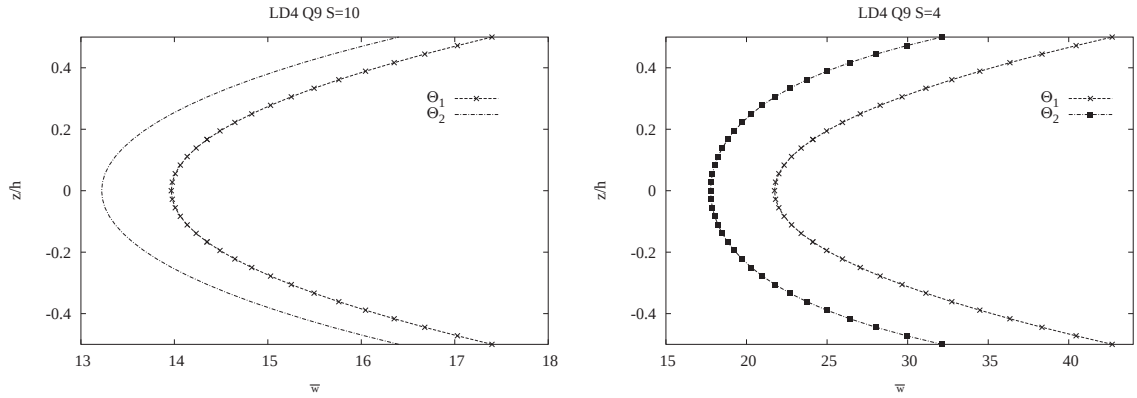

(a) $\bar{w}(\frac{a}{2}, \frac{b}{2})$ S=10 (b) $\bar{w}(\frac{a}{2}, \frac{b}{2})$ S=4

Figure 13: Comparison of the displacement-through-thickness distributions (u,v,w) between the linear (θ_1) and the actual (θ_2) temperature profile for two different side-to-thickness ratios (S=4 and S=10)

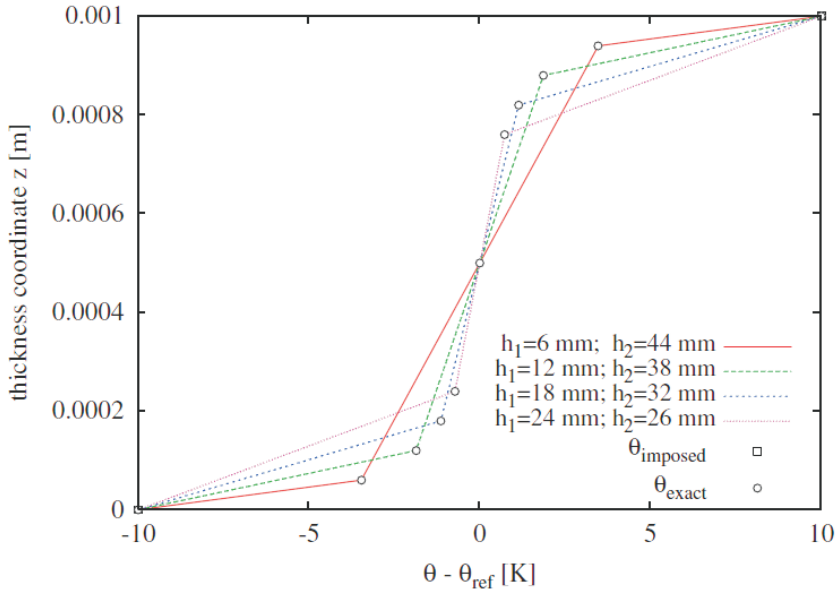

Figure 14: Variation of the plate-thickness temperature profile with the ratio h_1/h_2, total thickness constant - point $(\frac{a}{2}, \frac{a}{2})$

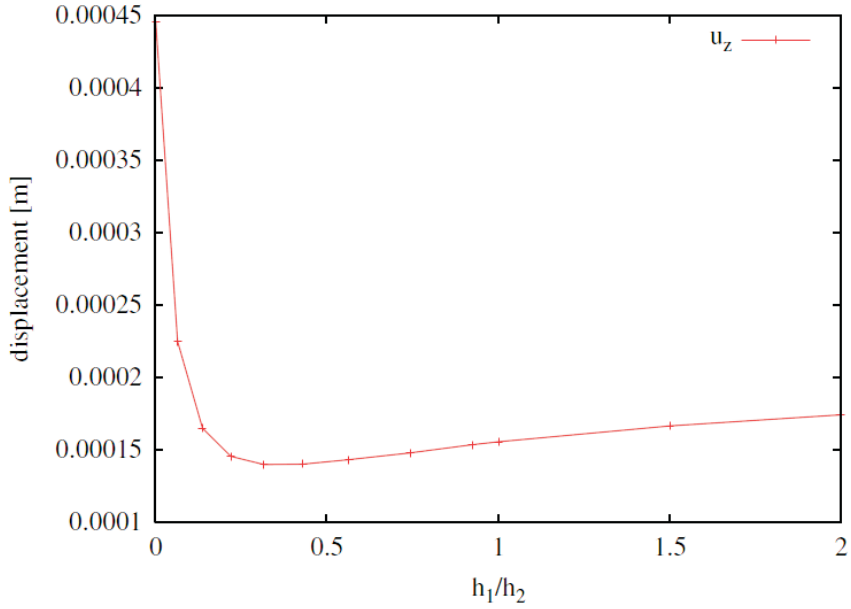

Figure 15: Variation of the displacement uz with the ratio h_1/h_2, total thickness constant - middle plate point

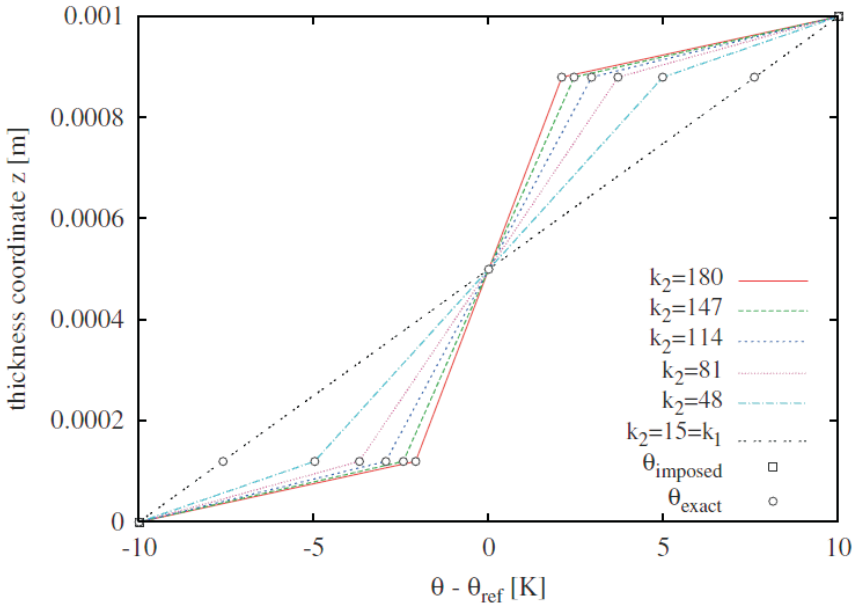

Figure 16: Variation of the plate-thickness temperature profile with the ratio κ_2/κ_1, κ_1 constant - point $(\frac{a}{2}, \frac{a}{2})$